AD-A280 990

NAVAL POSTGRADUATE SCHOOL
Monterey, California

THESIS

AN INVESTIGATION OF
THE TRANSONIC PRESSURE DRAG COEFFICIENT
FOR AXI-SYMMETRIC BODIES

by

Eddy Priyono

March, 1994

Thesis Advisor: Oscar Biblarz

DTIC QUALITY INSPECTED 3

94-20400

94 7 5 113

DISCLAIMER NOTICE

REPORT DOCUMENTATION PAGE

Form Approved OMB No. 0704

1. AGENCY USE ONLY *(Leave blank)*	2. REPORT DATE March 1994.	3. REPORT TYPE AND DATES COVERED Master's Thesis	
4. TITLE AND SUBTITLE AN INVESTIGATION OF THE TRANSONIC PRESSURE DRAG COEFFICIENT FOR AXI-SYMMETRIC BODIES		5. FUNDING NUMBERS	
6. AUTHOR(S) Eddy Priyono			
7. PERFORMING ORGANIZATION NAME(S) AND ADDRESS(ES) Naval Postgraduate School Monterey CA 93943-5000		8. PERFORMING ORGANIZATION REPORT NUMBER	
9. SPONSORING/MONITORING AGENCY NAME(S) AND ADDRESS(ES)		10. SPONSORING/MONITORING AGENCY REPORT NUMBER	

11. SUPPLEMENTARY NOTES The views expressed in this thesis are those of the author and do not reflect the official policy or position of the Department of Defense or the U.S. Government.

12a. DISTRIBUTION/AVAILABILITY STATEMENT Approved for public release; distribution is unlimited.	12b. DISTRIBUTION CODE *A

13.
ABSTRACT *(maximum 200 words)*

This thesis investigates the pressure drag coefficient in the transonic regime over an axi-symmetric body, with a set of unique contour surfaces developed in a previous thesis. The contour surfaces were obtained by an exact solution of the small perturbation transonic equation, using the guidelines and tools developed at NPS. In this work, Computational Fluid Dynamics (CFD) was not only used to compute the afterbody contour surface, but also to investigate a conical afterbody and complete bodies, which are composed of an arbitrary forebody (ellipsoid) and a variable afterbody (contour and conical). Euler as well as Navier-Stokes flow-solvers were applied to the geometries of interest, giving Mach-number contours for viscous and inviscid flow, pressure drag coefficient magnitude, and depicting shock wave location. On the basis of these results, it can be verified that our contour surface afterbodies will decrease by 15% the peak of the pressure drag coefficient (C_d) versus Mach number curves in the transonic regime. These results can be used to design low pressure drag surfaces for such as missiles, projectiles and aircraft engine nacelles.

14. SUBJECT TERMS Transonic pressure drag coefficient for axi-symmetric bodies.			15. NUMBER OF PAGES 94
			16. PRICE CODE
17. SECURITY CLASSIFICATION OF REPORT Unclassified	18. SECURITY CLASSIFICATION OF THIS PAGE Unclassified	19. SECURITY CLASSIFICATION OF ABSTRACT Unclassified	20. LIMITATION OF ABSTRACT UL

NSN 7540-01-280-5500

Standard Form 298 (Rev. 2-89)
Prescribed by ANSI Std. 239-18

AN INVESTIGATION OF
THE TRANSONIC PRESSURE DRAG COEFFICIENT
FOR AXI-SYMMETRIC BODIES

by

Eddy Priyono
Major, Indonesian Air Force
Mechanical Engineer,
Institute Technology of Surabaya, 1979

Submitted in partial fulfillment
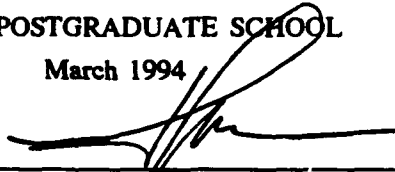of the requirements for the degree of

MASTER OF SCIENCE IN AERONAUTICAL ENGINEERING

from the

NAVAL POSTGRADUATE SCHOOL
March 1994

Author: _____
Eddy Priyono

Approved by: _____
Oscar Biblarz, Thesis Advisor

_____
Garth Hobson, Second Reader

_____
Daniel J. Colling, Chairman
Department of Aeronautics and Astronautics

ii

ABSTRACT

This thesis investigates the pressure drag coefficient in the transonic regime over an axi-symmetric body, with a set of unique contour surfaces developed in a previous thesis. The contour surfaces were obtained by an exact solution of the small perturbation transonic equation, using the guidelines and tools developed at NPS. In this work, Computational Fluid Dynamics (CFD) was not only used to compute the afterbody contour surface, but also to investigate a conical afterbody and complete bodies, which are composed of an arbitrary forebody (ellipsoid) and variable afterbody (contour and conical). Euler as well as Navier-Stokes flow-solvers were applied to the geometries of interest, giving Mach-number contours for viscous and inviscid flow, pressure drag coefficient magnitude, and depicting shock wave locations. On the basis of these results, it can be verified that our contour surface afterbodies will decrease by 15% the peak of the pressure drag coefficient (C_d) versus Mach number curves in the transonic regime. These results can be used to design low pressure drag surfaces for such shapes as missiles, projectiles and aircraft engine nacelles.

iii

TABLE OF CONTENTS

LIST OF TABLES

v

LIST OF FIGURES

vii

ACKNOWLEDGMENTS

I am particularly indebted and grateful to my thesis advisor, Prof. O. Biblarz, for his professional guidance and support throughout the development of this thesis; his unwavering commitment to the success of this task was thoroughly appreciated. I would like also to acknowledge the comments and suggestions made by Prof. G. Hobson on the CFD section to complete this thesis. Special thanks to my commanders in the Indonesian Air Force who gave me an opportunity to take the graduate program at NPS.

Finally, I want to thank my most understanding wife, Susy, my son Doddy and my daughter Meirina, for their great support and love that allowed me to contribute my best effort to do this thesis.

I. INTRODUCTION

The flight of an object over a wide range of speeds has a critical transition zone where both subsonic and supersonic types of flow exist. This speed regime is referred to as the transonic range. The critical aerodynamic behavior occurs in the range $0.8 < M < 1.2$ depending on the object, where the aerodynamic coefficients have been found to change by as much as 100%. The behavior of the aerodynamic force components is usually characterized by a rapid increase in the coefficients followed by a sharp drop, in other words, a peak value for the coefficients arises in this regime [Ref.1 and 2].

One of the aerodynamic components, aerodynamic drag, represents a significant adverse force on all flying objects such as aircraft, missiles and projectiles. A high drag force reduces the craft's range capability or equivalently requires more energy to achieve a certain range. Any effort to reduce the drag coefficient in the design process must concentrate on reducing the wake and pressure drag (inclusive of wave drag) contributions to the total drag.

A traditional approach to investigate aerodynamic characteristics is based on wind tunnel data and actual flight testing as a source for improvement of configurations to get the best results. Unfortunately, both wind tunnel and flight tests are considerably expensive and time consuming,

1

particularly in the transonic flow regime. Because of the great lateral influence of profiles at transonic speeds (shock reflection of the wall bounces back to the model), models must be made extremely small compared with wind tunnel dimensions and this introduces great experimental difficulties. Consequently, the data obtained at transonic speeds is considerably less reliable than at either subsonic or supersonic speeds. In addition, from a mathematical point of view, even the two dimensional small perturbation potential equation for transonic flow retains one non-linear term which is essential for non-divergent solutions at Mach one, but this non-linear partial differential equation has proven to be difficult to solve. Such inherent difficulties, coupled with the presence of shocks in the flow which cause boundary layer separation, have resulted in the creation of many approximate methods of solution which are employed in the design of transonic airfoils and the like [Ref.3, 4 and 5]. On the other hand, the use of numerical simulation known as Computational Fluid Dynamics (CFD) to predict aerodynamic characteristics greatly increases possibilities to improve design optimization at relatively low cost and allows for ease of design changes.

Finally, using the latest capabilities of Euler as well as Navier-Stokes flow-solvers, it has been possible to compute the flow over axi-symmetric bodies with various contours in the transonic regime.

II TRANSONIC FLOW

Transonic flows are characterized by the simultaneous presence within the flow field of both subsonic and supersonic regions. The properties of transonic flows can be derived from the general equations of gas dynamics, namely, the equations of state, continuity, momentum and energy. The following derivation based on assumptions that the flow is steady, irrotational and isentropic with no energy transfer, no body forces and no shear stresses (inviscid flow).

1. Small Perturbation Theory

Starting with the equation of motion for steady, isentropic, inviscid flow in the index notation form [Ref.4]:

$$u_i u_j \frac{\partial u_i}{\partial x_j} = a^2 \frac{\partial u_k}{\partial x_k} \tag{1}$$

Small-Perturbation Theory gives the velocity field as

$$u_1 = U + u \quad ; \quad u_2 = v \quad ; \quad u_3 = w \tag{2}$$

where U denotes the free stream velocity in the x direction and u, v, w are called perturbation velocity components in the direction x, y, z respectively.

Writing eq.(1) out in full, and substituting the velocity field eq.(2), gives the equation in terms of perturbation velocities.

$$a^2\left(\frac{\partial u}{\partial x} + \frac{\partial v}{\partial y} + \frac{\partial w}{\partial z}\right) = (U+u)^2\frac{\partial u}{\partial x} + v^2\frac{\partial v}{\partial y} + w^2\frac{\partial w}{\partial z}$$
$$+ (U+u)\,v\left(\frac{\partial u}{\partial y} + \frac{\partial v}{\partial x}\right) + vw\left(\frac{\partial v}{\partial z} + \frac{\partial w}{\partial y}\right) + w(U+u)\left(\frac{\partial w}{\partial x} + \frac{\partial u}{\partial z}\right)$$

(3)

From the energy equation for a perfect gas, the speed of sound (a) can be expressed in terms of the perturbation velocities.

$$\frac{(U+u)^2 + v^2 + w^2}{2} + \frac{a^2}{(\gamma-1)} = \frac{U^2}{2} + \frac{a_\infty^2}{(\gamma-1)}$$

(4)

or

$$a^2 = a_\infty^2 - \frac{(\gamma-1)}{2}(2uU + u^2 + v^2 + w^2)$$

(5)

Substituting eq.(5) into eq.(3), dividing by a_∞^2, and rearranging the terms, gives the full exact equation in terms of perturbation velocities and free stream Mach number. This equation contains linear terms on the left-hand side, but on the right-hand side the terms are nonlinear.

4

$$(1-M_\infty^2)\frac{\partial u}{\partial x} + \frac{\partial v}{\partial y} + \frac{\partial w}{\partial z} =$$

$$M_\infty^2\left[(\gamma+1)\frac{u}{U} + \frac{(\gamma+1)}{2}\frac{u^2}{U^2} + \frac{(\gamma-1)}{2}\frac{(v^2+w^2)}{U^2}\right]\frac{\partial u}{\partial x}$$

$$+ M_\infty^2\left[(\gamma-1)\frac{u}{U} + \frac{(\gamma+1)}{2}\frac{v^2}{U^2} + \frac{(\gamma-1)}{2}\frac{(w^2+u^2)}{U^2}\right]\frac{\partial v}{\partial y} \qquad (6)$$

$$+ M_\infty^2\left[(\gamma-1)\frac{u}{U} + \frac{(\gamma+1)}{2}\frac{w^2}{U^2} + \frac{(\gamma-1)}{2}\frac{(u^2+v^2)}{U^2}\right]\frac{\partial w}{\partial z}$$

$$+ M_\infty^2\left[\frac{v}{U}\left(1+\frac{u}{U}\right)\left(\frac{\partial u}{\partial y}+\frac{\partial v}{\partial x}\right) + \frac{w}{U}\left(1+\frac{u}{U}\right)\left(\frac{\partial u}{\partial z}+\frac{\partial w}{\partial x}\right) + \frac{vw}{U^2}\left(\frac{\partial w}{\partial y}+\frac{\partial v}{\partial z}\right)\right]$$

If the perturbation velocities are small ($u/U, v/U, w/U \ll 1$), eq.(6) can be simplified by neglecting the terms containing squares of the perturbation velocities on the right hand side, yielding :

$$(1-M_\infty^2)\frac{\partial u}{\partial x} + \frac{\partial v}{\partial y} + \frac{\partial w}{\partial z} =$$

$$M_\infty^2(\gamma+1)\frac{u}{U}\frac{\partial u}{\partial x} + M_\infty^2(\gamma-1)\frac{u}{U}\left(\frac{\partial v}{\partial y}+\frac{\partial w}{\partial z}\right) \qquad (7)$$

$$+ M_\infty^2\frac{v}{U}\left(\frac{\partial u}{\partial y}+\frac{\partial v}{\partial x}\right) + M_\infty^2\frac{w}{U}\left(\frac{\partial u}{\partial z}+\frac{\partial w}{\partial x}\right)$$

For further simplification, in eq. (7) all the terms on the right hand side can be neglected, in comparison to those on the left hand side. This gives the linear equation, which contains only perturbation velocities and is valid only for subsonic and supersonic flow.

$$(1-M_\infty^2)\frac{\partial u}{\partial x} + \frac{\partial v}{\partial y} + \frac{\partial w}{\partial z} = 0 \qquad (8)$$

For transonic flow, where $M_\infty \rightarrow 1$, the coefficient of $\partial u/\partial x$ on the left hand side becomes very small, but it is not correct to neglect the first term on the right hand side of eq. (7). Therefore, the governing equation of transonic flow in term of perturbation velocities is as follows:

$$(1-M_\infty^2)\frac{\partial u}{\partial x} + \frac{\partial v}{\partial y} + \frac{\partial w}{\partial z} = M_\infty^2 (\gamma+1) \frac{u}{U}\frac{\partial u}{\partial x} \qquad (9)$$

For irrotational flow, a perturbation velocity potential ϕ exists,

$$u = \frac{\partial \varphi}{\partial x}, \quad v = \frac{\partial \varphi}{\partial y}, \quad w = \frac{\partial \varphi}{\partial z} \qquad (10)$$

Substitution of eq. (10) into eq. (9), gives the governing equation for transonic flow in terms of the velocity potential.

6

$$(1-M_\infty^2) \frac{\partial^2 \varphi}{\partial x^2} + \frac{\partial^2 \varphi}{\partial y^2} + \frac{\partial^2 \varphi}{\partial z^2} = \frac{M_\infty^2 (\gamma+1)}{U} \frac{\partial \varphi}{\partial x} \frac{\partial^2 \varphi}{\partial x^2} \qquad (11)$$

For bodies of revolution, it is convenient to use cylindrical coordinates (x, r, θ) where x is aligned with the body axis. The velocity components corresponding to (x, r, θ) are u_x, u_r and u_θ, respectively. The velocity potential in the cylindrica coordinates,

$$u_x = U + u = \frac{\partial \phi}{\partial x} , \qquad u_r = \frac{\partial \phi}{\partial r} , \qquad u_\theta = \frac{1}{r} \frac{\partial \phi}{\partial \theta} \qquad (12)$$

Transforming Cartesian coordinate eq.(9) into cylindrical coordinate, gives the governing equation of transonic flow.

$$(1-M_\infty^2) \frac{\partial^2 \phi}{\partial x^2} + \frac{\partial^2 \phi}{\partial r^2} + \frac{1}{r} \frac{\partial \phi}{\partial r} + \frac{1}{r^2} \frac{\partial^2 \phi}{\partial \theta^2} = \frac{M_\infty^2 (\gamma+1)}{U} \frac{\partial \phi}{\partial x} \frac{\partial^2 \phi}{\partial x^2} \quad (13)$$

For axially symmetric flow, where the conditions are the same in every meridian plane, there is no variation with θ, so the small perturbation, non-linear, axi-symmetric transonic potential equation can be written as follows :

$$\frac{\partial^2 \phi}{\partial r^2} + \frac{1}{r} \frac{\partial \phi}{\partial r} + (1-M_\infty^2) \frac{\partial^2 \phi}{\partial x^2} = \frac{M_\infty^2 (\gamma+1)}{U} \frac{\partial \phi}{\partial x} \frac{\partial^2 \phi}{\partial x^2} \qquad (14)$$

7

Or rewriting in shorthand notation,

$$\phi_{rr} + \frac{1}{r}\phi_r + (1-M_\infty^2)\phi_{xx} = \frac{M_\infty^2(\gamma+1)}{U}\phi_x\phi_{xx} \qquad (15)$$

Reference 6 introduces a modified potential equation for axi-symmetric flows

$$\frac{1}{r}\frac{\partial}{\partial r}(r\phi_r) + (1-M_\infty^2)\phi_{xx} = \phi_x\phi_{xx} \qquad (16)$$

where the modified velocity potentials are :

$$\phi_x = M_\infty^2(\gamma+1)\frac{u_x}{U} \ , \qquad \phi_r = M_\infty^2(\gamma+1)\frac{u_r}{U} \qquad (17)$$

2. An exact solution for axi-symmetric, transonic flow.

Solutions to the modified transonic eq.(16) have been given by Biblarz [Ref.6 and 7] by using the separation of variables approach with a potential function $\phi(x,r)$ of the form

$$\phi(x,r) = \xi(x)\eta(r) + (1-M_\infty^2)x \qquad (18)$$

Substituting the above ϕ function in the modified transonic eq.(16) results in two ordinary, second order, non-linear differential equations

8

$$\frac{d\xi}{dx}\frac{d^2\xi}{dx^2} - \lambda\xi = 0 \qquad (19)$$

and

$$\frac{d^2\eta}{dr^2} + \frac{1}{r}\frac{d\eta}{dr} - \lambda\eta^2 = 0 \qquad (20)$$

where λ is the separation constant.

The solution to the first differential eq.(19) is obtained by multiplying both sides $d\xi/dx$,

$$\frac{d\xi}{dx}\left[\frac{d\xi}{dx}\frac{d^2\xi}{dx^2}\right] - \frac{d\xi}{dx}(\lambda\xi) = 0 \qquad (21)$$

or

$$\frac{d}{dx}\left[\frac{1}{3}\left(\frac{d\xi}{dx}\right)^3 - \frac{\lambda}{2}\xi^2\right] = 0 \qquad (22)$$

Thus

$$\frac{d\xi}{dx} = \left(\frac{3}{2}\lambda\xi^2 + \alpha\right)^{\frac{1}{3}} \qquad (23)$$

where α is a constant given by Ref.6.
Rearranging eq.(23)

$$dx = \frac{d\xi}{\left(\frac{3}{2}\lambda\xi^2 + \alpha\right)^{\frac{1}{3}}} \qquad (24)$$

9

and integrating eq.(24) gives,

$$x - x_0 = \int \frac{d\xi}{\left(\frac{3}{2}\lambda\xi^2 + \alpha\right)^{\frac{1}{3}}} \tag{25}$$

where α and x_0 are integration constants.

The solution to the second non-linear ordinary differential equation (20), is obtained by an outer expansion method. [Ref.8]

$$\eta(r) = \frac{4}{\lambda r^2} + (1-M_\infty^2) f_1(r) + (1-M_\infty^2)^2 f_2(r) + \ldots \tag{26}$$

Where $(1-M_\infty^2)$ represents a small parameter and the first term is the purely sonic solution.

By taking first and second derivatives eq.(26) and subtituting them into eq.(20) yields,

$$\eta(r) = \frac{1}{\lambda r^2}\left[4 + |1-M_\infty^2| a\lambda r^{(\sqrt{8}+2)} + \frac{(1-M_\infty^2)^2}{28+8\sqrt{8}} a^2\lambda^2 r^{2(\sqrt{8}+2)} + \ldots\right] \tag{27}$$

Al-Hashel [Ref.9] reported on eq.(26) and eq.(27), implemented the boundary conditions with the constants α, C_1, a and λ, gave the final results in the new variables,

$$\tilde{\xi} = \xi\left[\frac{3\lambda}{2C_1}\right]^{\frac{1}{2}} \tag{28}$$

10

$$\tilde{r}^{(\sqrt{8}+2)} = r^{(\sqrt{8}+2)} \lambda a \tag{29}$$

$$\tilde{x} = C_1^{-\frac{1}{6}} x \left(\frac{3\lambda}{2}\right)^{\frac{1}{2}} \tag{30}$$

$$\tilde{\eta} = \frac{\eta \lambda}{(a\,\lambda)^{0.4142}} \tag{31}$$

then

$$\tilde{x} = \int \frac{d\tilde{\xi}}{\left[\tilde{\xi}^2 + |1-M_\infty^2|^{1.7574}\right]^{\frac{1}{3}}} \tag{32}$$

where $x_0 = 0$, and

$$\tilde{\eta} = \frac{1}{\tilde{r}^2}\left[4 + |1-M_\infty^2|\; \tilde{r}^{(\sqrt{8}+2)} + \frac{(1-M_\infty^2)^2}{50.63}\tilde{r}^{2(\sqrt{8}+2)}\right] \tag{33}$$

Equation (32) has been numerically integrated and plotted on figure (1) as $\xi(\tilde{x})$ versus $\tilde{x}$, and eq.(33) will be evaluated and plotted in figure (2) as $\tilde{\eta}(\tilde{r})$ versus $\tilde{r}$ for $M_\infty = 1.05$, 1.1 and 1.2. A "patching" technique discussed in Ref.9 has been used here.

11

III. PRESSURE COEFFICIENT AND BOUNDARY SURFACES

1. Pressure Coefficient

Liepmann and Roshko [Ref.4] define the pressure coefficient as,

$$C_p = \frac{(p-p_\infty)}{0.5\rho_\infty U^2} = \frac{2}{\gamma M_\infty^2} \left[\frac{p}{p_\infty} - 1\right] \tag{34}$$

From the isentropic relation, we have pressure ratio in terms of Mach number and after substituting into eq.(34) yields

$$C_p = \frac{2}{\gamma M_\infty^2} \left[\left[\frac{2+(\gamma-1)M_\infty^2}{2+(\gamma-1)M^2}\right]^{\gamma/(\gamma-1)} - 1 \right] \tag{35}$$

Introducing $M_\infty^2 = U^2/a_\infty^2$, $M^2 = u^2/a^2$ and using energy equation (recall eq.4 and eq.5), the pressure coefficient can be expressed in terms of the perturbation velocities,

$$C_p = \frac{2}{\gamma M_\infty^2} \left\{ \left[1 + \frac{\gamma-1}{2}M_\infty^2\left(1 - \frac{(U+u)^2+v^2+w^2}{U^2}\right)\right]^{\gamma/(\gamma-1)} - 1 \right\} \tag{36}$$

$$= \frac{2}{\gamma M_\infty^2} \left\{ \left[1 - \frac{\gamma-1}{2}M_\infty^2\left(\frac{2u}{U} + \frac{u^2+v^2+w^2}{U^2}\right)\right]^{\gamma/(\gamma-1)} - 1 \right\}$$

Using the binomial expansion on the expression inside the square brackets in eq.(36), we obtain the pressure coefficient in the form

$$C_p = - \left[\frac{2u}{U} + (1 - M_\infty^2) \frac{u^2}{U^2} + \frac{v^2 + w^2}{U^2} \right] \tag{37}$$

For axi-symmetric flow, in cylindrical coordinates where $u = u_x$ and $(v^2 + w^2) = u_r^2$, substituting into eq.(37) yields

$$C_p = - \left[\frac{2u_x}{U_\infty} + (1 - M_\infty^2) \left(\frac{u_x}{U_\infty} \right)^2 + \left(\frac{u_r}{U_\infty} \right)^2 \right] \tag{38}$$

The linearized pressure coefficient approximation for axi-symmetric flow turns out to be

$$C_p = - \frac{2u_x}{U_\infty} \tag{39}$$

Recall the modified axial velocity potential, eq.(17),

$$\phi_x = M_\infty^2 (\gamma + 1) \frac{u_x}{U_\infty} \tag{40}$$

thus

$$\frac{u_x}{U_\infty} = \frac{\phi_x}{M_\infty^2 (\gamma + 1)} \tag{41}$$

Substitute eq.(41) into eq.(39), yields

$$C_p = \frac{-2 \phi_x}{M_\infty^2 (\gamma+1)} \tag{42}$$

The derivative of the potential function eq.(18) with respect to x becomes

$$\phi_x = \eta \frac{d\xi}{dx} + (1-M_\infty^2) \tag{43}$$

Ref.6 introduces relation of the constants C_1, α, a and λ in expression,

$$\alpha = \pm C_1 |1-M_\infty^2|^{1.7574} \tag{44}$$

and

$$\left(\frac{C_1}{\lambda}\right) \frac{a^{1.2426}}{\lambda^{0.7574}} = 1.08 x 10^{-2} \tag{45}$$

Rewriting eq.(23) and substitute the constant α eq.(44) becomes

$$\frac{d\xi}{dx} = \left[\frac{3\lambda}{2}\xi^2 + C_1 |(1-M_\infty^2)|^{1.7574} \right]^{\frac{1}{3}} \tag{46}$$

14

Recall the new variable eq.(28)

$$\tilde{\xi} = \xi \left[\frac{3\lambda}{2C_1} \right]^{\frac{1}{2}} \qquad (47)$$

Substituting eq.(47) into eq.(46) and factoring C_1 out, yields

$$\frac{d\xi}{dx} = C_1^{\frac{1}{3}} \left[\tilde{\xi}^2 + | (1-M_\infty^2) |^{1.7574} \right]^{\frac{1}{3}} \qquad (48)$$

Recall and arrange new variable eq.(31)

$$\eta = \frac{(a\,\lambda)^{0.4142}}{\lambda} \tilde{\eta} \qquad (49)$$

Rewriting eq.(43) the modified potential function and inserting eq.(48) and eq.(49), becomes

$$\phi_x = \frac{(a\lambda)^{0.4142}}{\lambda} \tilde{\eta} \, C_1^{\frac{1}{3}} \left[\tilde{\xi}^2 + | (1-M_\infty^2) |^{1.7574} \right]^{\frac{1}{3}} + (1-M_\infty^2) \qquad (50)$$

or

$$\phi_x = \frac{a^{0.4142} C_1^{\frac{1}{3}}}{\lambda^{0.5858}} \tilde{\eta} \left[\tilde{\xi}^2 + | (1-M_\infty^2) |^{1.7574} \right]^{\frac{1}{3}} + (1-M_\infty^2) \qquad (51)$$

15

Substituting the expression of constants eq.(45) into eq.(51)

$$\phi_x = 0.2208 \, \bar{\eta} \left[\bar{\xi}^2 + | (1-M_\infty^2) |^{1.7574} \right]^{\frac{1}{3}} + (1-M_\infty^2) \qquad \textbf{(52)}$$

Finally, rewriting the pressure coefficient C_p as

$$C_p = \frac{-2}{M_\infty^2 (\gamma+1)} \left[0.2208 \bar{\eta} \left[\bar{\xi}^2 + | (1-M_\infty^2) |^{1.7574} \right]^{\frac{1}{3}} + (1-M_\infty^2) \right] \qquad \textbf{(53)}$$

2. Boundary Surfaces

For an inviscid flow, the condition to be applied at the surface of a solid boundary is that the direction of the flow velocity vector must be tangent to the solid surface. In other words, the velocity vector is everywhere at right angles to the normal to the solid boundary [Ref.10]. In addition the boundary condition requires that the gradient of potential ϕ vanish far ahead of the body. In terms of perturbation velocities this boundary condition becomes

$$\left(\frac{dr}{dx} \right)_{surface} = \frac{u_r}{U_\infty} \qquad \textbf{(54)}$$

16

Recall the modified velocity perturbation potential eq.(17)

$$\phi_r = M_\infty^2 \ (\gamma+1) \frac{u_r}{U_\infty} \qquad (55)$$

thus

$$\frac{u_r}{U_\infty} = \frac{\phi_r}{M_\infty^2 \ (\gamma+1)} \qquad (56)$$

substituting eq.(56) into eq.(54),

$$\left(\frac{dr}{dx}\right) = \frac{\phi_r}{M_\infty^2 \ (\gamma+1)} \qquad (57)$$

Taking the differential of eq.(18) with respect to r gives

$$\phi_r = \xi \ \frac{d\eta}{dr} \qquad (58)$$

Expressing eq.(58) in terms of new variables, recall eq.(28), eq.(29) and eq.(31)

$$\phi_r = 0.0848 \ \tilde{\xi} \ \frac{d\tilde{\eta}}{d\tilde{r}} \qquad (59)$$

17

Recalling eq.(33) and taking the derivative with respect to $\tilde{r}$, then substituting eq.(59) into eq.(57), yields

$$\left(\frac{d\tilde{r}}{dx}\right) = \frac{0.0848}{M_\infty^2(\gamma+1)}\xi\left[\frac{-8}{\tilde{r}^3}+2.8284\ |1-M_\infty^2|\ \tilde{r}^{1.8284}+0.1512(1-M_\infty^2)^2\ \tilde{r}^{6.657}\right]$$

(60)

Replacing the left hand side of eq.(60) with the new variables eq.(29) and eq(30), then rearranging it becomes

$$\frac{d\tilde{r}}{d\tilde{x}} = \frac{0.0326}{M_\infty^2(\gamma+1)}\xi\left[\frac{-8}{\tilde{r}^3}+2.8284\ |1-M_\infty^2|\ \tilde{r}^{1.8284}+0.1512(1-M_\infty^2)^2\ \tilde{r}^{6.657}\right]$$

(61)

For further arrangement, by separating variables eq.(61), yields

$$\frac{d\tilde{r}}{\left[\dfrac{8}{\tilde{r}^3}-2.8284|1-M_\infty^2|\ \tilde{r}^{1.8284}-0.1512(1-M_\infty^2)^2\ \tilde{r}^{6.657}\right]} =$$

$$\frac{-0.0326}{M_\infty^2(\gamma+1)}\ \xi\ d\tilde{x}$$

(62)

Then, integrating both sides of eq.(62) becomes

18

$$\int_{\tilde{r}_0}^{\tilde{r}} \frac{d\tilde{r}}{\left[\dfrac{8}{\tilde{r}^3} - 2.8284|1-M_\infty^2|\,\tilde{r}^{1.8284} - 0.1512(1-M_\infty^2)^2\,\tilde{r}^{6.657}\right]} =$$

$$\frac{-0.0326}{M_\infty^2(\gamma+1)} \int_0^{\tilde{x}} \xi\, d\tilde{x} \qquad (63)$$

where

$$\tilde{r}_0 = \frac{1.2074}{|1-M_\infty^2|^{0.2071}} \qquad (64)$$

Al-hashel [Ref.10] has developed and computed eq.(63) using numerical integration, to determine the boundary surfaces in dimensional and non-dimensional (normalized) form for M_∞ = 1.05, 1.10 and 1.20 as depicted in Figure (3) and Figure (4). Based on these calculations, the geometric grid of the afterbody for Mach number 1.10 and 1.20 are developed for further study with Computational Fluid Dynamic (CFD).

This thesis research also examines conical afterbodies as a solid afterbody boundary surface with base diameter ratio (d_b/d_m) of 0.50 and 0.75 and conical turning angle (β) of 26.6 and 14.0 degree respectively [Ref.11 and 12]. Then, for further investigation, the complete bodies as a solid boundary surface are generated, with a kind of forebody (ellipsoid) joined with the contour surface afterbodies a; well as the conical afterbodies.

IV. DRAG

Drag is one of the aerodynamic force components parallel to free stream velocity (U_∞). It represents a significant adverse force on all flying objects. Basically, the drag force is divided into two categories, the drag caused by forces acting normal to the boundary surface which is called pressure drag (inclusive forebody, base and wave drag) and that arising from the tangential forces acting on the surface, by virtue of viscosity which is called viscous drag or skin friction. Figure (5) shows the components of the drag as function of Mach number and the methods used to compute body drag in four Mach number regimes [Ref.5].
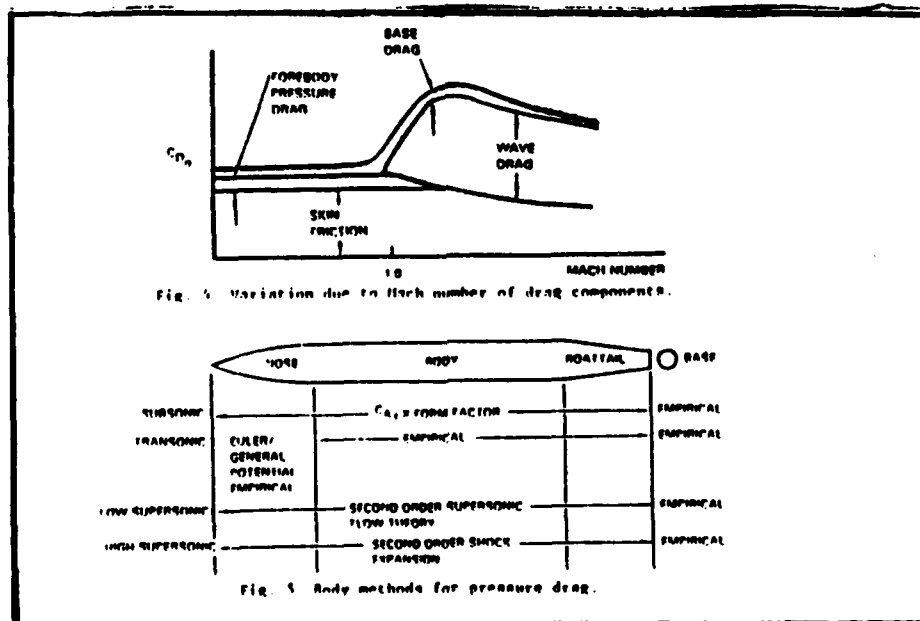
Figure 5.   Components of the Drag [Ref.5]

20

1. Skin Friction

Skin friction is the result of shearing force within the boundary layer of a viscous flow, acting tangentially to a surface in motion relative to the fluid. The amount of viscous resistance depends upon whether the flow is laminar or turbulent [Ref.5]. Krasnov [Ref.13] introduces the laminar and turbulent skin friction for flat plates, based on the boundary layer theory, for compressible flow. These formulas also valid for bodies of revolution with infinite length.

Laminar flow, $Re < 10^6$:

$$C_{fL} = \frac{1.32}{(Re)^{\frac{1}{2}}} (1 + 0.03M_{\infty}^2)^{-\frac{1}{3}} \tag{65}$$

Turbulent flow, $Re > 10^6$:

$$C_{fT} = \frac{0.472}{(1+0.1M_{\infty}^2)} \left[\log_{10}Re \ (1+0.2M_{\infty}^2)^{-1.76} \right]^{-2.58} \tag{66}$$

where Re is the Reynold number

21

2. Pressure Drag

Liepmann and Roshko [Ref.4] introduce the pressure drag formula (inclusive wave drag and base drag) for axi-symmetric bodies as,

$$D = \int_0^L p \, dS - p_B S(L)$$

$$= \int_0^L (p-p_\infty) \, dS + (p_\infty-p_B) S(L)$$

(67)

or, in dimensionless form,

$$C_D = \frac{D}{q_\infty S(L)}$$

(68)

$$= \frac{1}{S(L)} \left[\int_0^L C_p \frac{dS}{dx} dx + C_{pB} \right]$$

where $S(x) = \pi r^2$ is the cross-sectional area of the body at x.

$$dS(x) = 2\pi r dr = 2\pi r \frac{dr}{dx} dx \qquad (69)$$

or

$$\frac{dS}{dx} = 2\pi r \frac{dr}{dx} \qquad (70)$$

The first term in square bracket eq.(68) can be solved by inserting eq.(53), eq.(60) and eq.(70) yielding,

$$\int_0^L C_p \frac{dS}{dx} = \int_0^L \left\{ \left[\frac{-2}{M_\infty^2(\gamma+1)} \left[0.2208\tilde{\eta} \left[\tilde{\xi}^2 + | (1-M_\infty^2)|^{1.7574} \right]^{\frac{1}{3}} + (1-M_\infty^2) \right] \right] \right\}$$

(71)

$$(2\pi r) \left\{ \frac{0.0326}{M_\infty^2(\gamma+1)} \tilde{\xi} \left[\frac{-8}{\tilde{r}^3} + 2.8284 | 1-M_\infty^2 | \tilde{r}^{1.8284} + 0.1512(1-M_\infty^2)^2 \tilde{r}^{6.657} \right] \right\} dx$$

Recalling new variables eq.(28), eq.(29), eq.(30) and inserting $\beta^2 = 1-M_\infty^2$ into eq.(71) yields,

$$\int_0^L C_p \frac{dS}{dx} dx =$$

$$\int_0^{\tilde{x}} \left\{ \left[\frac{-2}{(1-\beta^2)(\gamma+1)} \left[0.2208\tilde{\eta} \left[\tilde{\xi} + | \beta^{3.5148} | \right] \right]^{\frac{1}{3}} + \beta^2 \right] \right\} \left[\frac{5.1302 C_1^{\frac{1}{6}}}{\lambda^{0.7071} a^{0.2071}} \right]$$

(72)

$$\left\{ \frac{0.0326}{(1-\beta^2)(\gamma+1)} \tilde{\xi} \left[\frac{-8}{\tilde{r}^3} + 2.8284 | \beta^2 | \tilde{r}^{1.8284} + 0.1512 \beta^4 \tilde{r}^{6.657} \right] \right\} d\tilde{x}$$

where C_1, a and λ are constants.

23

The second term in square bracket eq.(68) is the contribution to the drag by the base pressure p_B. Ref.4 claims, that the values of the base pressure coefficient C_{pB} must be obtained experimentally. However Krasnov [Ref.13] introduces the boattail drag coefficient for a conical afterbody as,

$$C_{pB} = 0.002 \left[0.8 + \frac{1}{M_\infty^2} \right] \delta^{1.7} (1 - \bar{S}_B) \tag{73}$$

where :

δ = turning angle of the conical body

$\bar{S}_B$ = ratio of the base area to the mid-section area

In this work, the skin friction coefficient as well as the pressure drag coefficient of the geometries of interest, at specified Mach number, can be obtained directly from the results of CFD calculations. The Euler solution will give the pressure drag and the Navier-Stokes solution will give both.

24

V. COMPUTATIONAL FLUID DYNAMICS

The rapid advancement in the speed of computers and their enormous memory size has led to the emergence of the field of computational fluid dynamics (CFD). This branch of fluid dynamics complements its experimental and theoretical branches, by providing an alternate, cost-effective means of simulating real flow. It also offers the only means of examining theoretical advances for conditions unavailable experimentally. As a model based method, CFD can provide the convenience of being able to switch off specific terms in the governing equations [Ref.14], so as to assist the researcher in understanding the contributions of various physical factors.

In this work, CFD was used to compute the axi-symmetric flow over the afterbody geometry of models only (the boundary surfaces obtained by the small perturbation method [Ref.9] and conical afterbody) and over complete body models which are composed of forebody (ellipsoid) and afterbody.

1. Grid Generation

The computer programs GRAPE [Ref.15] and GRIDGEN2D [Ref.16] are tools used to generate two-dimensional structured grids about airfoils and other shapes by the use of algebraic or Poisson differential equation solvers. GRAPE was used for

the geometry with smooth contour surfaces, while GRIDGEN2D was used for the geometry with a conical afterbody with non-smooth points. Outer and inner boundaries were specified as the C-type grid for afterbody models only, while the O type grid was for the complete body models, where both type of grids treat the surface of the body as the inner boundary. The important characteristics in a grid generation technique are the ability to specify the spacing between mesh points at the boundary, in the direction normal to the boundary, and the control of the angles with which mesh lines intersect the boundaries which is known as orthogonality [Ref.15].

Figure (6) is a typical output of program GRAPE for an afterbody with small perturbation solution contour for Mach 1.10 (SPS_1.1), C-type grid with the grid size of 115x60, and figure (7) is the complete body with the grid size of 152x60 (O-type grid).

To develop a three-dimensional grid from two-dimensional grid (output program GRAPE), the FORTRAN code called HALF.F (Appendix) was used to write out the half of the 2D grid and convert them into 3D plane-grid. Then, the FORTRAN code ROTATEGR.F (Appendix) was used to rotate the 3D plane-grid for 11 planes plus 2 more to generate a 3D volume grid of half of an axi-symmetric body surface as shown in figure (8) and figure (9) with grid size of 58x13x60 and 77x13x60 respectively. These grids are ready for further processing with a flow-solver.

Program GRIDGEN2D gives the pattern of how to build 2D-grid. It consists of four subfaces which are treated as boundaries. Grid spacing is determined by setting up the distribution points of each pair subfaces. It uses equal spacing along the body surface, while the direction normal to the body surface uses geometric spacing with specified width in the beginning. Figure (10) and Figure (11) are typical outputs of GRIDGEN2D for an afterbody and for a complete body with the grid size of 58x60 and 77x60 respectively. FORTRAN code D2D3.F (Appendix) is used to convert 2D grid output from GRIDGEN2D into 3D plane-grid. Then we apply the FORTRAN code ROTATEGR.F to generate a 3D volume grid of half of an axi-symmetric body as depicted in Figure (12) and Figure (13) with the grid size of 58x13x60 and 77x13x60.

In this research, we also attempted to develop a fine grid for complete bodies (O-type grid), where the radius of outer boundary is set up to be five times of the body's length. The steps to obtain 3D volume grid are similar to those described above with the final grid size of 77x9x120 and the final geometry of a quarter of an axi-symmetric body instead of a half body. Figures (14) and (15) are typical fine grids of the complete body with a conical afterbody and a complete body with contour surface afterbody.

2. Flow-solver

The OVERFLOW program [Ref.17] was developed by NASA·Ames Research Center. It uses either 3-D Euler or Navier-Stokes flow-solvers for inviscid/viscous flow, by setting True or False the parameter VISINP (viscosity input) in the input file (overflow.in). Before flow-solver code (OVERFLOW) is applied on the grid file, a formatted 3D grid file named "grid.for" must be converted into an unformatted grid file named "grid.in", by using FORTRAN code called READX.F (Appendix). Then, the NAMELIST input file parameter specification must be written for running OVERFLOW, it is called "overflow.in". The input parameter consists of the number of iterations, timesteps, calculation methods, smoothing, type of flow and boundary conditions for each grid. The value of angle of attack (ALPHA) depends on the orientation of the grid in the coordinate system. In this case, ALPHA is 180° (flow comes from the x-positive to the x-negative direction). The boundary conditions depend on the geometry corresponding to the final 3D volume grid. Both input parameters, the angle of attack and the boundary conditions for each geometric shape, are tabulated in Table 1.

The file overflow.in (Appendix) is a typical input parameter specification of the axi-symmetric body with a conical afterbody using the grid size of 77x13x60. This file input uses NSTEP=100, Mach number=0.95, ALPHA=180°. The calculation method depends on a central difference Euler term

28

in J, K, L and ARC3D diagonal factorization and dissipation scheme (IRHS=0, ILHS=2, IDISS=2). For the first attempt a time step DT=0.1, ITIME=1 and CFLMIN=5.0 was utilized. The boundary condition consists of 6 boundaries (NBC=6), with the type of BC IBTYP=30 (inflow) in the J positive (1), IBTYP=15 (Axis K round) in J negative (-1) direction, IBTYP=12 (symmetry in Y) in the K positive (2) and K negative (-2) direction, IBTYP=1 (Inviscid adiabatic wall) in the L positive (3) direction and IBTYP=32 (Supersonic /subsonic inflow/outflow) in the L negative (-3) direction.

The OVERFLOW program gives output files such as ovr.out, q.save, resid.out and fomo.out. To verify that a calculation is appropriate or converged, it can be traced by looking at the plot of residual history (resid.out). A convergence criterion was defined as the reduction in residuals by two orders of magnitude. If the first run (NSTEP=100) does not fulfill the convergence criterion, one may perform a restart by further running OVERFLOW and changing the parameter RESTART=.T. in the input file (overflow.in) and by copying q.save into q.restart. Repeating the above steps until all convergence criteria are met. If in the output file q.bomb appears, one tries another run by changing parameter time step DT and CFLMIN until the criteria are met. Then, one converts the output file q.save (unformatted) into formatted file named q.form by using FORTRAN code READ1.F (Appendix).

Finally, the last step is to run PLOT3D program with the

source formatted files x=grid.for and q=q.form. By using functions on the PLOT3D program, many plots such as pressure, velocity, Mach number, vorticity, etc., are obtained.

3. Results

The results of CFD programs are grouped into the corresponding geometric shape, namely, afterbody only and complete body. The Euler flow-solver (inviscid flow) was applied to all axi-symmetric bodies, except for the afterbody models only, where both Euler and Navier-Stokes (viscous flow) were applied. Most of the calculations converged in 500 iterations, meaning that the residual history achieved a two order of magnitude drop.

Results can be analyzed by plotting the q.form file, output file from the OVERFLOW program, using the proper function in PLOT3D program (Mach number). By interpreting the Mach number contour surrounding the body surfaces, one can be determine the characteristics of the flow field. In addition, the drag coefficient C_d, can be obtained in the file fomo.out, output from OVERFLOW. Hence, in the sequences of Mach number, one can describe the significant flow characteristic of each geometric shape.

a. Afterbodies

An Euler as well as a Navier-Stokes flow-solver was applied to these afterbody models. The approaching free stream

Mach number (ranging from 1.05 to 1.50) starts from the mid-section of the afterbodies, then the flow follows along the afterbody surface until it reaches a maximum local Mach number as tabulated in Table 2. The maximum local Mach number for viscous flow is always lower compared to in the inviscid flow. This may be caused by the viscous flow itself since we are taking into account the shear force in the boundary layer near the surface.

For the afterbodies from the small perturbation solution contour (SPS1.0, SPS1.1 and SPS1.2), in inviscid flow, the shocks are formed at the contour surface. The location of the shock depends on the specific afterbody contour and the approaching Mach number; at the higher Mach numbers the shock appears a bit further downstream as shown in Figures (16) through (21). As shown in Figure (22) and Figure (23), this is apparently a result of viscosity; it shows the boundary layer by the increment of Mach number away form the surface. Weak shocks were formed further downstream compared to inviscid flow. Flow separation occurs in the starting contour region and is followed by circulating flow in the base region.

For the conical afterbody, the approaching free stream Mach number increases following the mid-section surface, then a flow expansion occurs at the turning angle region, until the maximum local Mach number is reached. A weak shock is formed at the end of the boattail region as shown in Figure (24), while for the viscous flow, the weak shock develops away from

31

boattail surface due to the boundary layer and the separation of the flow. The circulating flow in the base region is more significant than in the inviscid flow as depicted in Figure (25). In addition, from Table 2, for viscous flow the maximum local Mach number for the conical afterbody is higher than for the contoured afterbody.

For each afterbody the pressure drag coefficient (C_d) versus free stream Mach number (M_∞) for inviscid and viscous flow are plotted in Figure (26). The negative sign of C_d is due to the fact that the calculation of pressure starts from mid-section through the base of afterbody and ignores the forebody pressure. These results show that the pressure drag coefficient is higher for viscous flows than for inviscid flows for each given afterbody. This may be caused by the viscosity effect and the pressure distribution difference in the flow field. In addition, it can be seen from the chart, that the C_d for the afterbody with small perturbation solution contour Mach 1.10 (SPS1.1) has the lowest C_d values over the entire Mach number range. Therefore, the SPS1.1 contour shows to be relatively the best among these afterbodies.

b. **Complete Bodies**

Complete bodies consist of an arbitrary forebody (ellipsoid) joined to various afterbodies such as the small perturbation solution contours (SPS_1.1 and SPS_1.2) and a conical afterbody. The approaching free stream Mach number (M_∞

32

ranging from 0.50 to 1.50) starts from outer boundary with distance of 1 times for the coarse grid and 5 times body's length for the fine grid respectively. Significant differences between coarse and fine grid calculations can be seen from the characteristic bow shock. In the coarse grid, the bow shock hits the outer boundary, this causes the approaching free stream Mach number not to be the same as in the input parameter as shown in Figure (27). While in the fine grid, the bow shock dies out before reaches the outer boundary as depicted in Figure (28). So, further discussion is focused on the fine grid exclusively.

The flow stagnates on the nose and then follows the body surface until it reaches a maximum local Mach number as tabulated in Table 3. The critical Mach number for these complete bodies is approximately at $M_\infty = 0.70$, where the maximum local Mach number reaches unity at the shoulder region.

Figure (29) shows a typical high subsonic free stream Mach number ($M_\infty = 0.85$) flow over the complete body SPS_1.1. The flow stagnates on the nose tip, then flow is accelerated following the forebody surface reaching a sonic line at the mid-way of the forebody and forming a supersonic region at the shoulder. Then, the flow deccelerates at the mid-section and accelerates again until reaches a maximum local Mach number at the starting region of the afterbody and a weak shock occurs in this region. A supersonic approaching free stream Mach

33

number, is depicted in Figures (30) and (31) for SPS_1.1 and SPS_1.2 respectively. A bow shock is obviously seen in front of the nose. The characteristic of the bow shock is more inclined down stream for the higher M_∞ as shown in Figure (32). A subsonic region is formed between bow shock and the nose, then the flow accelerates along the forebody surface up to a supersonic region in the mid-section. The expansion flow occurs in the starting contour region until it reaches a maximum local Mach number. Then, a shock is formed in the contour region. Similar as in the afterbody only, the shock location depends upon the contour surface and M_∞. The shock location for a given contour is more downstream for higher M_∞ and at the same M_∞, the shock location for SPS_1.1 is more downstream than SPS_1.2. A typical residual history of CFD calculation for complete body with small perturbation solution contour is shown in Figure (33). Convergence is obtained at about 500 iterations.

For the conical afterbody, the flow characteristic is the same as the other complete bodies up to the mid-section region. The expansion flow occurs at the turning angle, then the flow accelerated along the conical surface and weak shock is formed at the edge of base. Figures (34) and (35) show the Mach number contour and corresponding residual calculation for conical afterbody at $M_\infty = 1.10$.

The pressure drag coefficient (C_d-press) versus free stream Mach number (M_∞) for fine grid complete bodies are

plotted in Figure (36). The drag rises sharply in the high subsonic Mach number ($M_\infty \approx 0.95$) and reaches a maximum (peak) at $M_\infty \approx 1.10$. Then the drag decreases with a shallow curve as the M_∞ increases. The decreasing shallow curve may be caused by the bluntness of the nose and it agrees with Shapiro [Ref.18] because the fineness ratio and bluntness of the nose of bodies of revolution are the important factors that contribute the drag curve at transonic and supersonic range. It can be seen from the graph, the drag curve of complete body with conical afterbody is higher than with small perturbation solution contour at the entire M_∞. Furthermore, the peak of the drag curve is approximately 15% higher. The drag curve for SPS_1.1 and SPS_1.2 are likely to have the same trend up to M_∞ = 0.95; beyond this Mach number, the drag curve for SPS_1.2 is slightly greater than for SPS_1.1. Therefore, the complete body with small perturbation solution contour afterbody Mach 1.1 (SPS_1.1) relatively gives the lowest drag.

VI. CONCLUSIONS AND RECOMMENDATIONS

The use of numerical simulation (CFD) appears to be the most cost effective method to predict the aerodynamic performance, especially in the transonic range.

In this research, the grid-generating program GRAPE is suitable only for the geometry with smooth contour surface (SPS_1.1 and SPS_1.2), while the program GRIDGEN2D is used for the geometry of a conical afterbody with non-smooth points.

We have shown that for a complete body model the use of a fine grid (77x9x120) is more reliable than a coarse grid (77x13x60). This is shown by the characteristic of the bow shock at $M_\infty > 1$ as seen in Figures 27 and 28. The pressure drag coefficient (C_d) versus free stream Mach number (M_∞) graphs show that the small perturbation solution contour for Mach 1.10 (SPS_1.1) gives relatively the lowest C_d on both models (afterbody and complete body), a decrease of approximately 15% of peak in the transonic range compared to the conical afterbody. Therefore, the best design of an axisymmetric body such as missiles, projectiles and aircraft, can be based on the small perturbation solution contour.

Finally, this work may be continued with the investigation a complete body with pointed nose geometry and the application of a Euler as well as Navier-Stokes flow-solvers within various small angle of attack.

36

LIST OF REFERENCES

1. Sahu, J., "Numerical Computations of Transonic Critical Aerodynamic Behavior," AIAA Journal, Vol 28 No.5, May 1990.

2. Sahu, J., "Three-Dimensional Base-Flow Calculation for a Projectile at Transonic Velocity," AIAA Journal, Vol. 27 No. 2, February 1989.

3. Guderley, K. G., "The Theory of Transonic Flow," Pergamon Press, London 1962.

4. Liepmann, H. W., Roshko, A., "Elements of Gas Dynamics," John Wiley and Sons, Inc., 1957.

5. Nixon, D., "Transonic Aerodynamics," AIAA, Progress in Astronautics and Aeronautics, Vol. 81, 1982.

6. Biblarz, O., "Phase Plane Analysis of Transonic Flows," AIAA, Paper No. 76-332, July 1976.

7. Biblarz, O., "An Exact Solution to the Transonic Equation," Israel Journal of Technology, Vol. 13, 1975.

8. Van Dyke, M.D., "Perturbation Methods in Fluid Mechanics," Academic Press, NY 1964.

9. Al-hashel, W.I., "Two-Dimensional Boundary Surfaces for Axi-Symmetric External Transonic Flows," MS Thesis, Naval Postgraduate School, 1993.

10. Zucrow, M. J., Hoffman, J. D. "Gas Dynamics," Vol. I & II, John Wiley and Sons, Inc., 1976.

11. Chow, W.L., "Base Pressure of a Projectile Within the Transonic Flight Regime," AIAA Journal, Vol.23, No.3, March 1985.

12. Payne, P.R., "Drag of Conical and Circular Arc Afterbodies Without Jet Flow," Aviation and Surface Effect Department, DTNSRDC/ASED-80/10, May 1980.

13. Krasnov, N.F., "Aerodynamics of Bodies of Revolution," American Elsevier Publishing Co., Inc., New York 1970.

14. Fletcher, C.A.J., "Computational Techniques for Fluid Dynamics," Vol I, Springer-Verlag, New York 1990.

15. Sorenson, R.L., "A Computer Program to Generate Two-Dimensional Grids About Airfoils and Other Shapes by the use of Poison's Equation," NASA Technical Memorandum 81198, 1981.

16. Steinbrenner,J.P., Chawner,J.R.,"The Gridgen V.8 Multiple Block Grid Generation Software," MDA Engineering, Inc., Arlington, Texas, December 1992.

17. Bunning, P.G., and others, "Overflow User's Manual Version 1.6g," NASA AMES Research Center, California, June, 1992.

18. Shapiro, A.H.,"The Dynamics and Thermodynamics of Compressible Fluid Flow," The Ronald Press Company, New York 1954.

TABLE 1. INPUT PARAMETER FOR OVERFLOW.i

Input	Afterbodies	Half complete bodies	Quarter complete bodies
GRID	56x13x60	77x13x60	77x9x120
ALPHA	180°	180°	180°
NBC	6	6	6
IBTYP	15,40,12,12, 1,32	15,15,12,12, 1,32	15,15,12,13, 1,32
IBDIR	1,-1, 2,-2, 3,-3	1,-1, 2,-2, 3,-3	1,-1, 2,-2, 3,-3
JBCS	1,58, 1, 1, 1, 1	1,77, 1, 1, 1, 1	1,77, 1, 1, 1, 1
JBCE	1,58,58,58,58,58	1,77,77,77,77,77	1,77,77,77,77,77
KBCS	1, 1, 1,13, 1, 1	1, 1, 1,13, 1, 1	1, 1, 1, 9, 1, 1
KBCE	13,13, 1,13,13,13	13,13, 1,13,13,13	9, 9, 1, 9, 9, 9
LBCS	1, 1, 1, 1, 1,60	1, 1, 1, 1, 1,60	1, 1, 1, 1, 1,120
LBCE	60,60,60,60, 1,60	60,60,60,60, 1,60	120,120,120,120,1,120

Note:

IBDIR = Coordinate direction of boundary condition (away form boundary surface).
1,2,3,-1,-2,-3 represent J,K,L,-J,-K,-L,respectively.

ALPHA = 180° (flow comes from x-positive to x-negative direction)

IBTYP =
1 : Inviscid adiabatic wall.
5 : Viscous adiabatic wall.
12 : Symmetry in Y.
13 : Symmetry in Z.
15 : Axis (K round).
30 : Outflow.
32 : Supersonic/subsonic inflow/outflow.
40 : Inflow

39

TABLE 2.   MAXIMUM LOCAL MACH # FOR AFTERBODIES

$Mach_\infty$	SPS_1.0		SPS_1.1		SPS_1.2		Conical	
	INV	VISC	INV	VISC	INV	VISC	INV	VISC
1.05	1.70	1.40	1.70	1.40	1.70	1.40	1.80	1.55
1.10	1.80	1.40	1.75	1.45	1.75	1.45	1.85	1.60
1.15	1.85	1.50	1.80	1.50	1.80	1.50	1.85	1.65
1.20	1.90	1.55	1.85	1.55	1.85	1.60	1.90	1.70
1.30	2.00	1.60	1.95	1.65	2.00	1.65	2.00	1.80
1.50	2.30	1.80	2.20	1.85	2.20	1.90	2.20	2.00

Note :

SPS_1.1 :   Small Perturbation Solution contour for Mach 1.1

INV   :   Inviscid flow

VISC   :   Viscous flow

40

TABLE 3. MAXIMUM LOCAL MACH NUMBER FOR COMPLETE BODY

GRID / M_∞	AFT-SPS_1.1		AFT-SPS_1.2		AFT-CONE1	AFT-CONE2	
	Coarse	Fine	Coarse	Fine	Coarse	Coarse	Fine
0.50	0.64	0.68	0.64	0.66	0.70	0.64	0.64
0.75	1.05	1.10	1.05	1.10	0.95	1.05	1.05
0.85	1.35	1.30	1.35	1.30	1.50	1.30	1.30
0.95	1.60	1.45	1.60	1.45	1.65	1.40	1.40
1.05	1.70	1.60	1.70	1.60	1.75	1.50	1.45
1.10	1.85	1.70	1.80	1.70	1.75	1.55	1.50
1.20	1.95	1.80	1.90	1.80	1.85	1.60	1.60
1.30	2.10	1.90	2.10	1.90	1.90	1.70	1.70
1.50	2.30	2.10	2.30	2.10	2.10	1.90	1.90
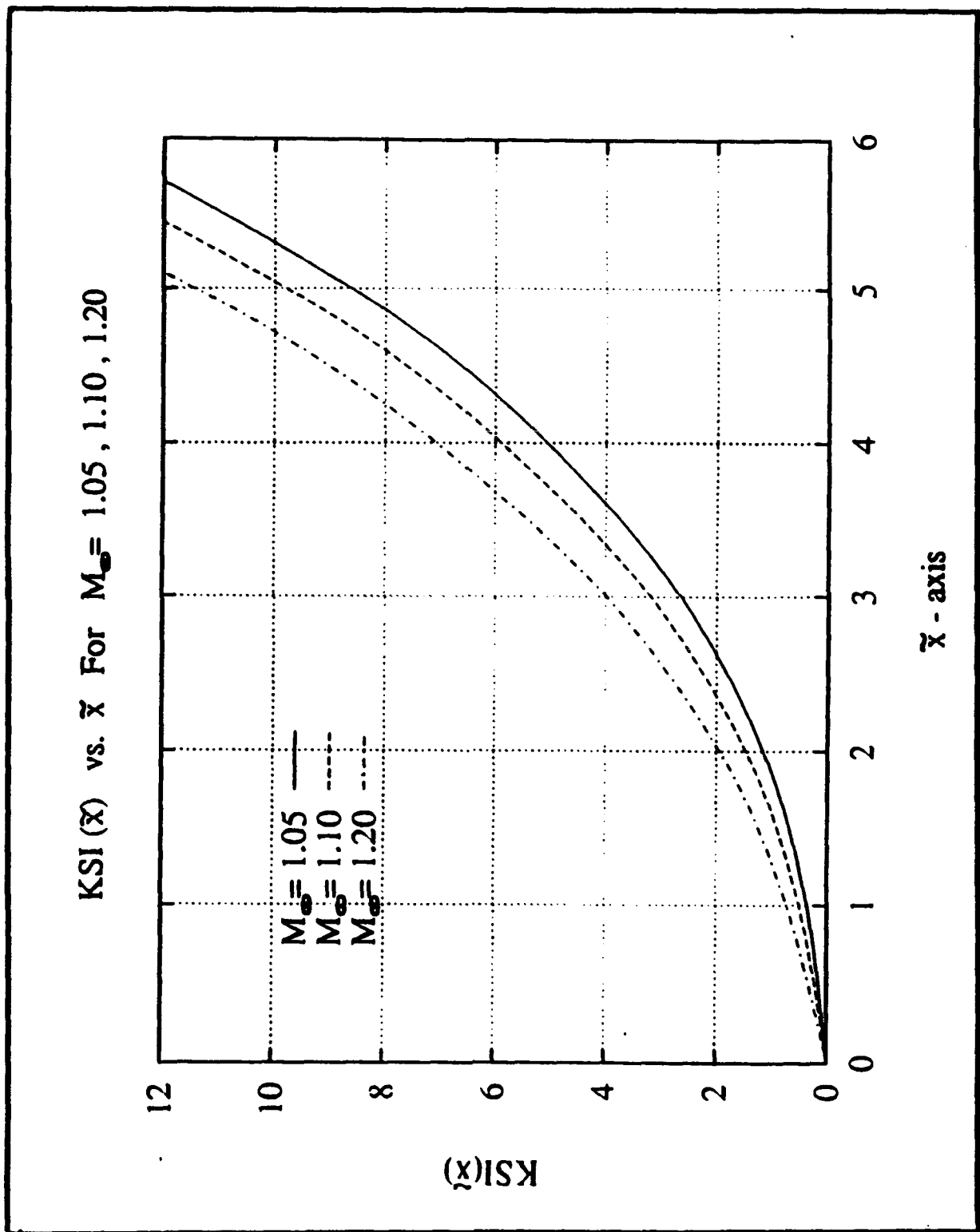
Figure 1. Numerical integration of equation (32).

Figure 2. Numerical solution of equation (33).

43

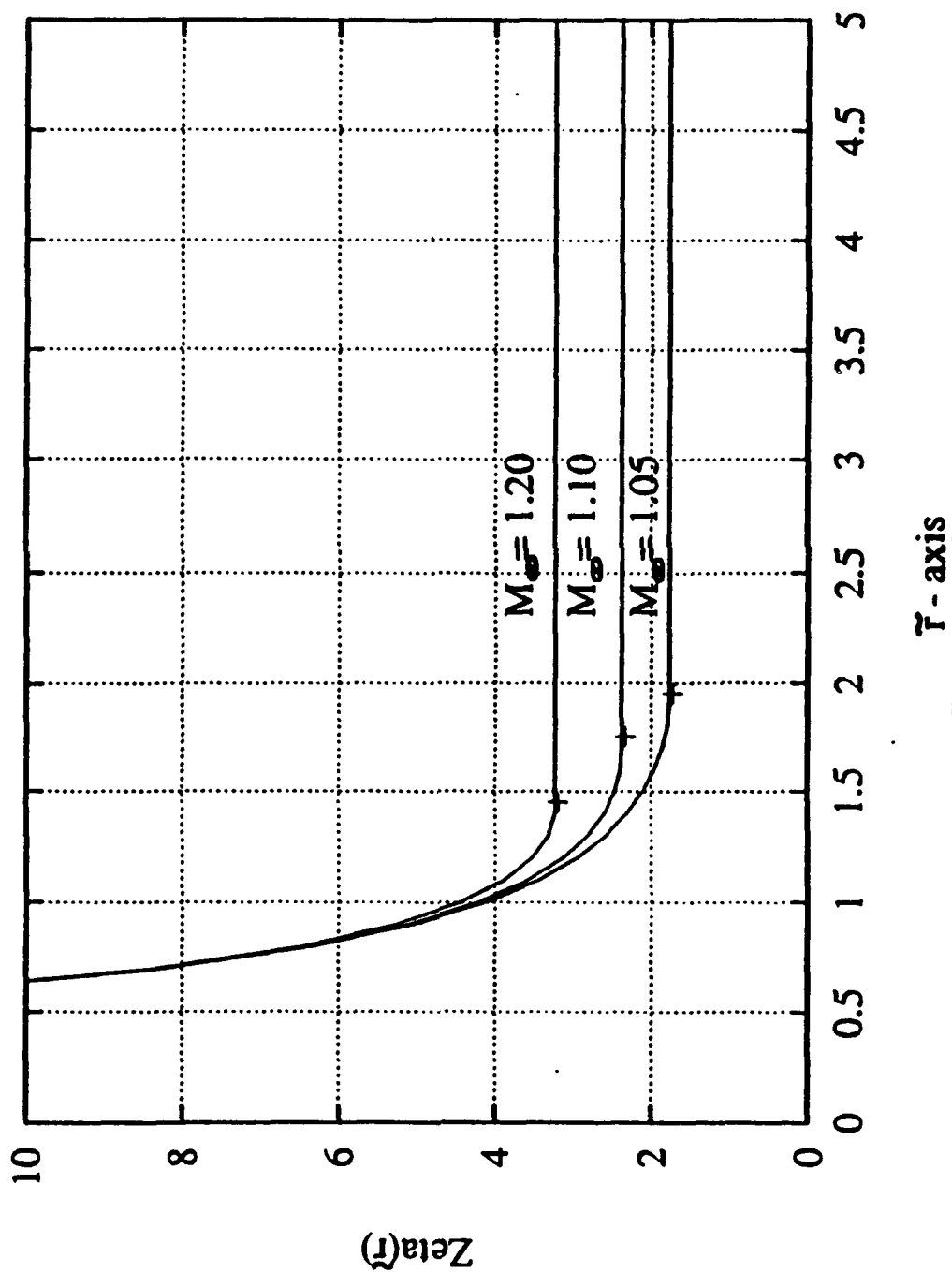SUPERSONIC BOUNDARY SURFACES

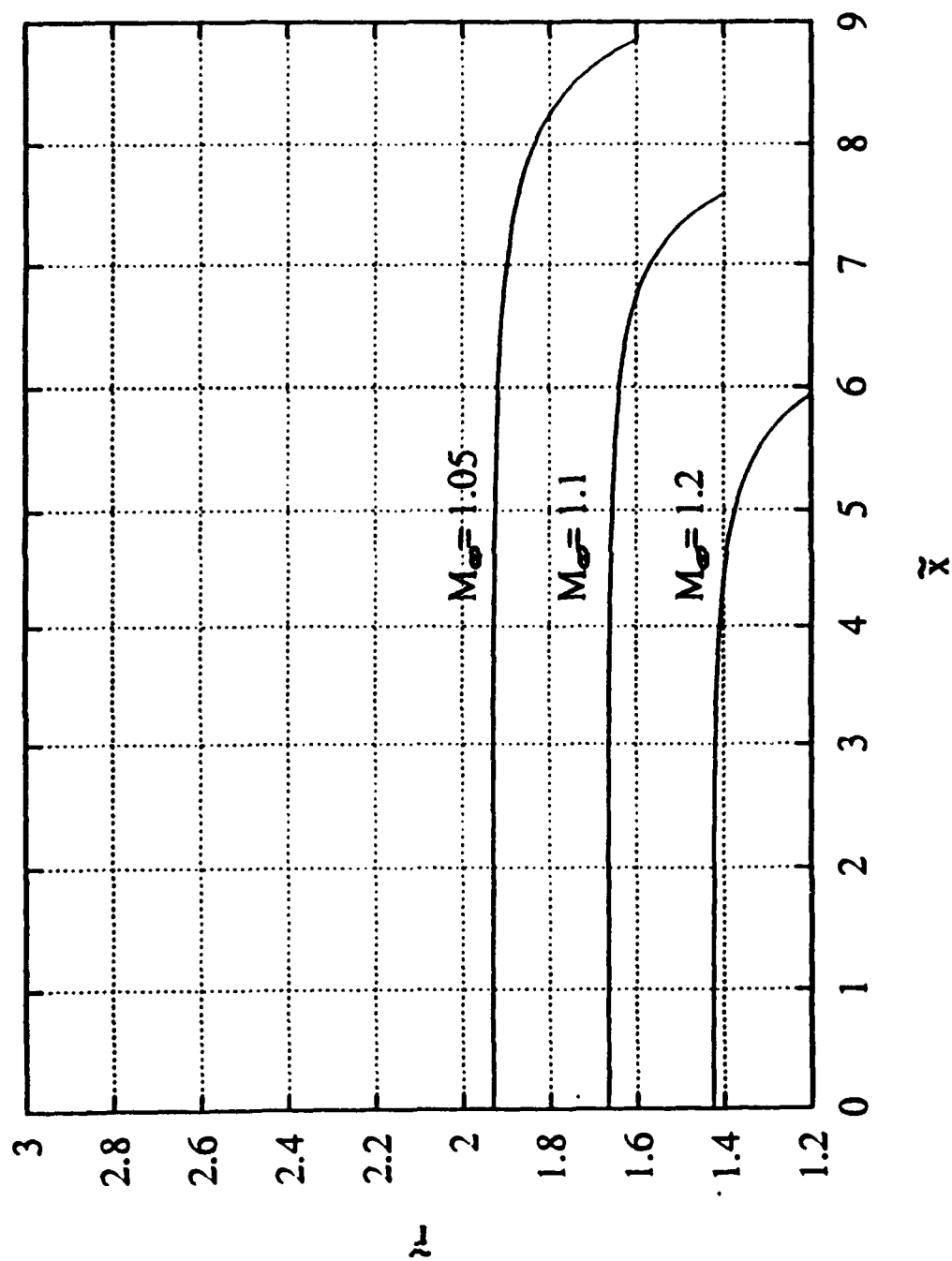$M_\infty = 1.05$

$M_\infty = 1.1$

$M_\infty = 1.2$

Figure 3. Numerical integration of equation (63).
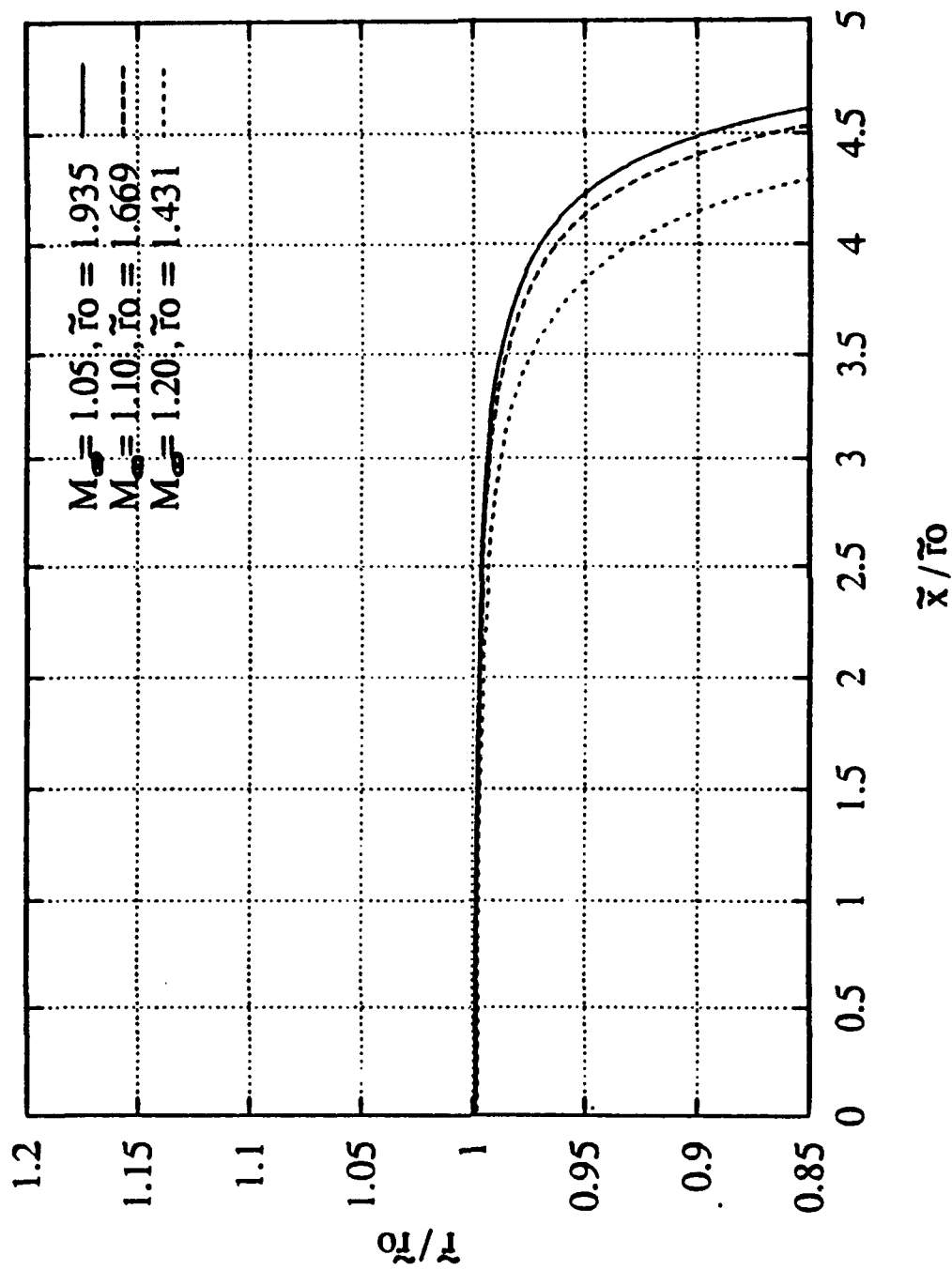
SUPERSONIC BOUNDARY SURFACES

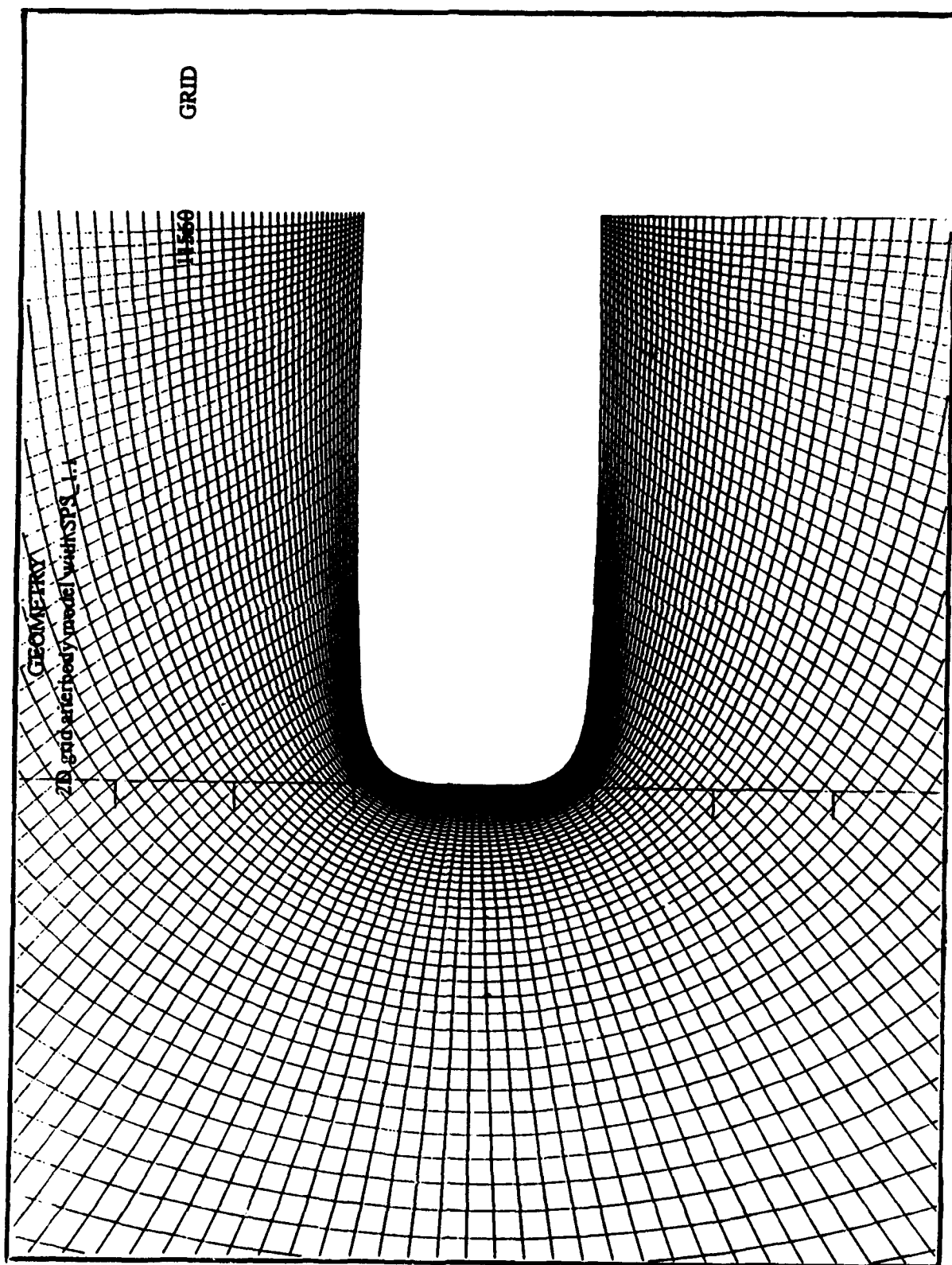Figure 4. Numerical integration of equation (63) (normalized)
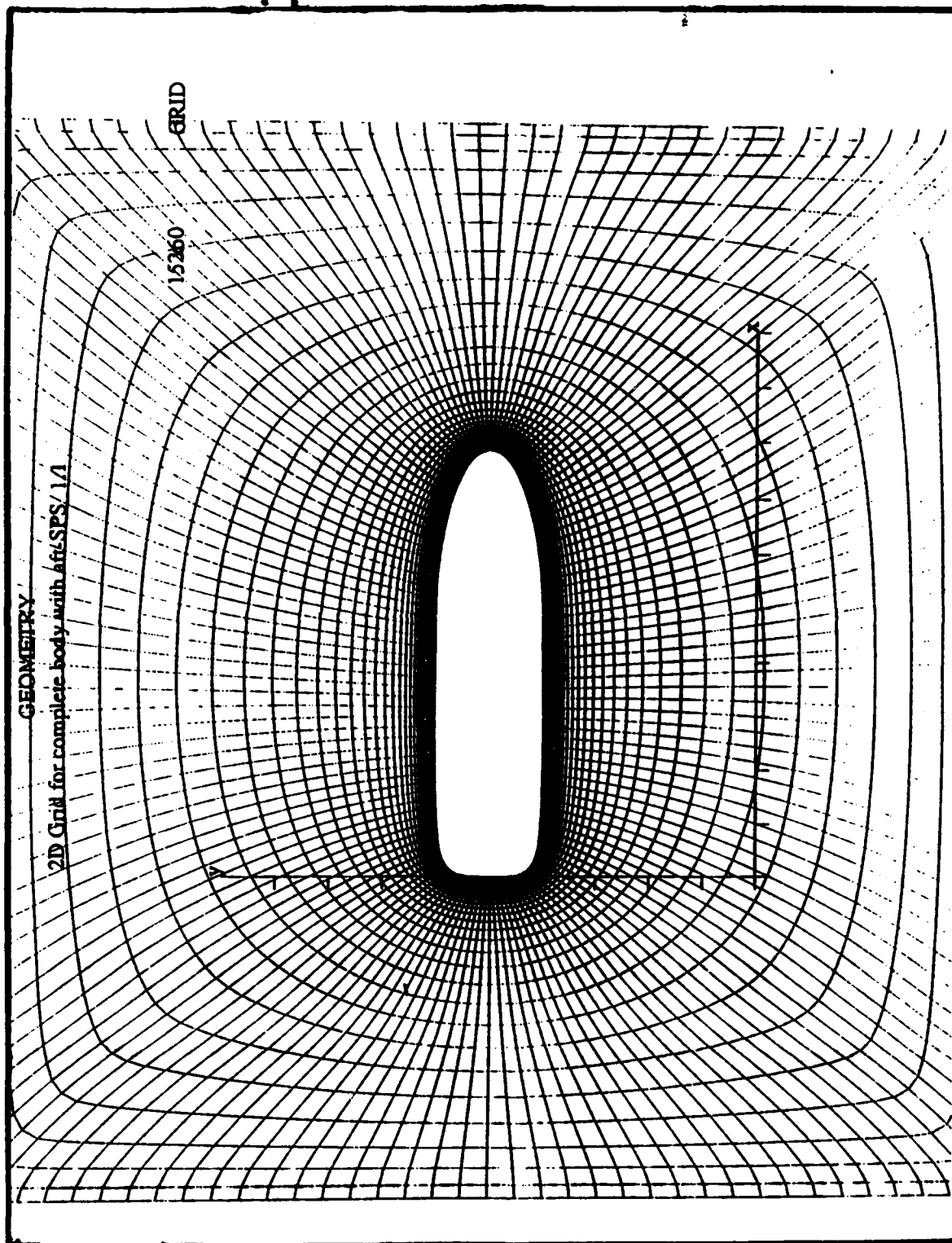
Figure 6. 2D grid , afterbody model with SPS_1.1
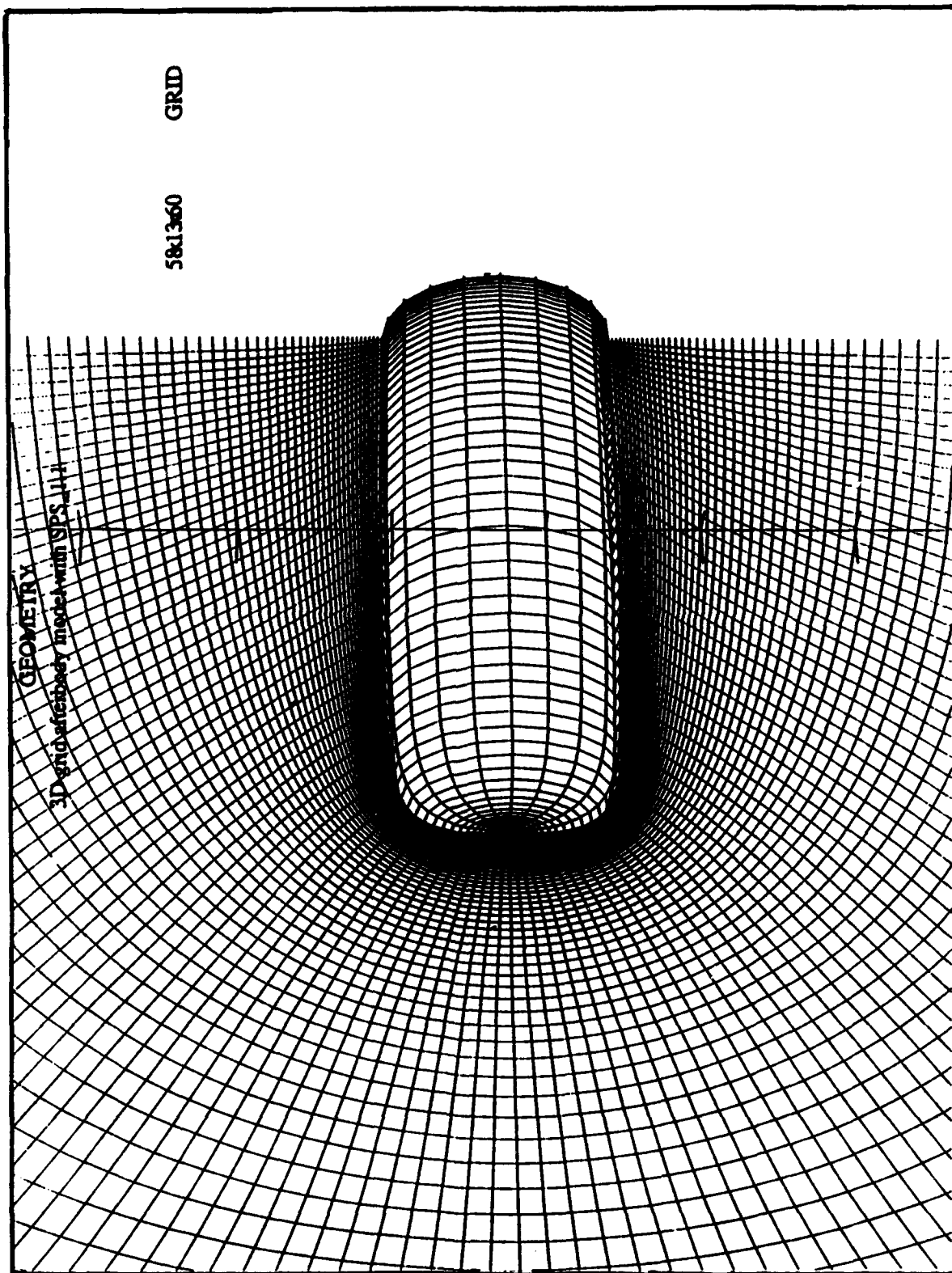
Figure 7. 2D grid, complete body with SPS_1.1.

Figure 8. 3D grid , afterbody model with SPS_1.1

48

GEOMETRY:
3D grid, complete body with SPS_1|1
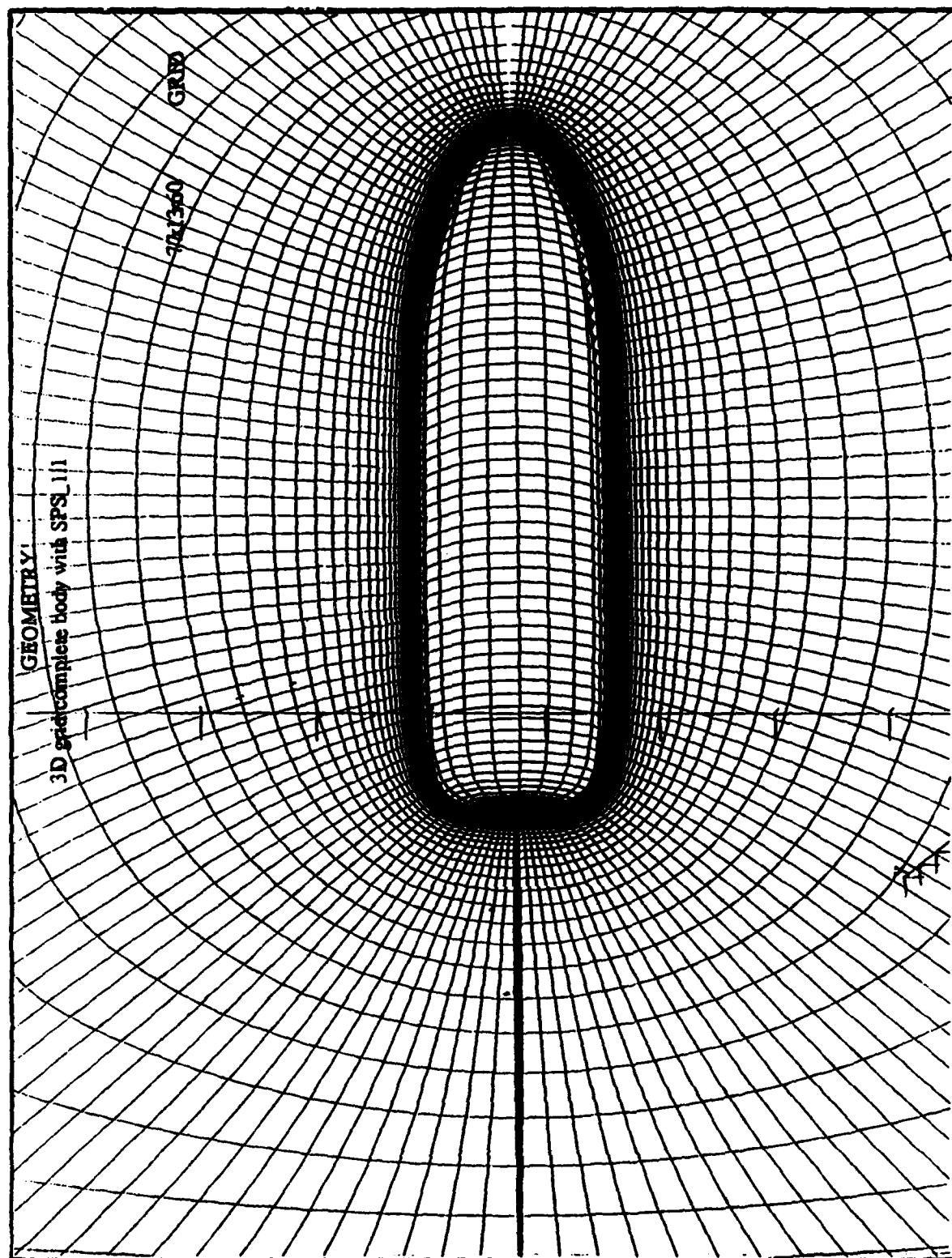
Figure 9. 3D grid, complete-body with SPS_1.1

49

Figure 10. 2D grid, conical afterbody model.

GRID

7x60

GEOMETRY

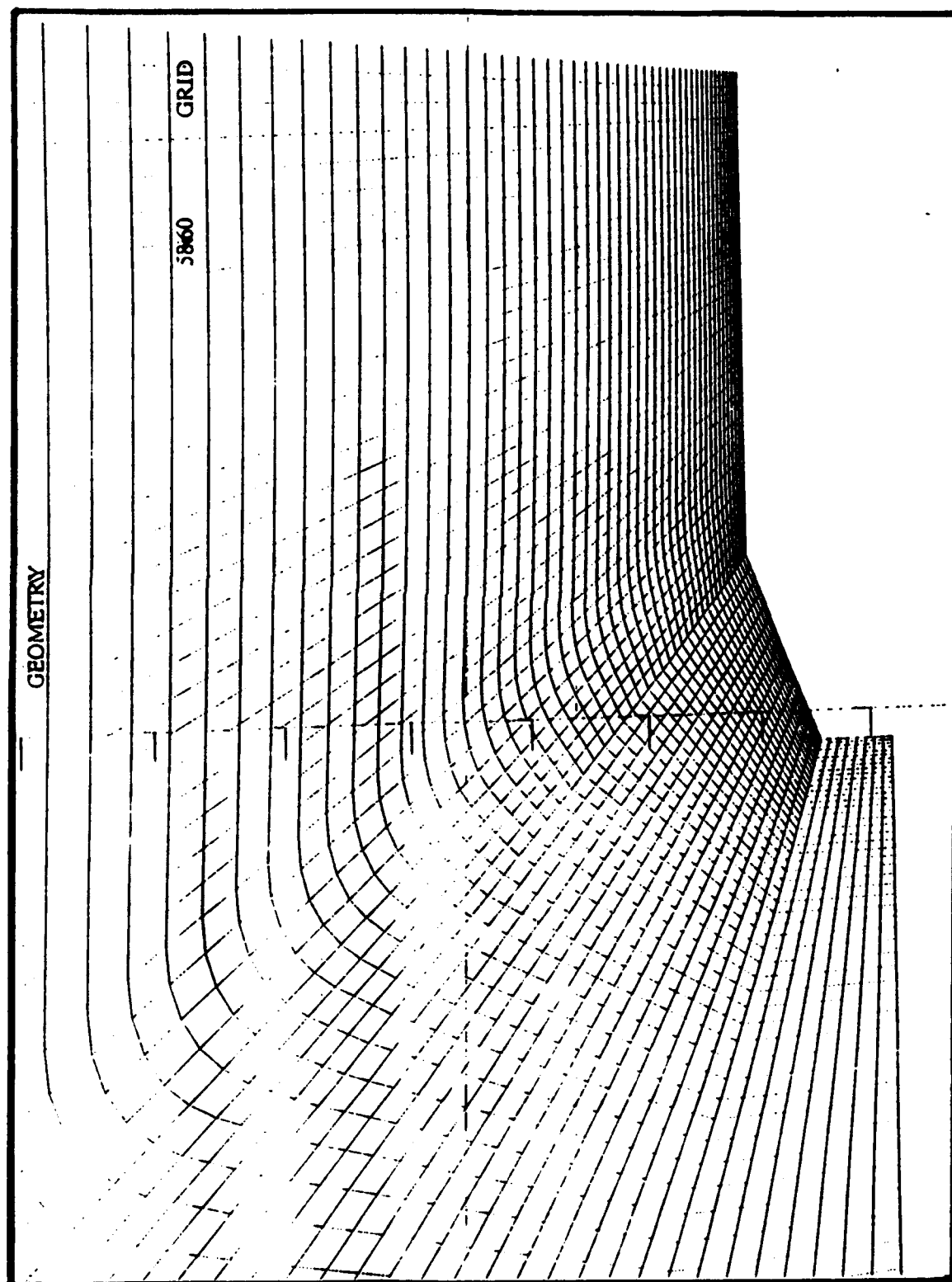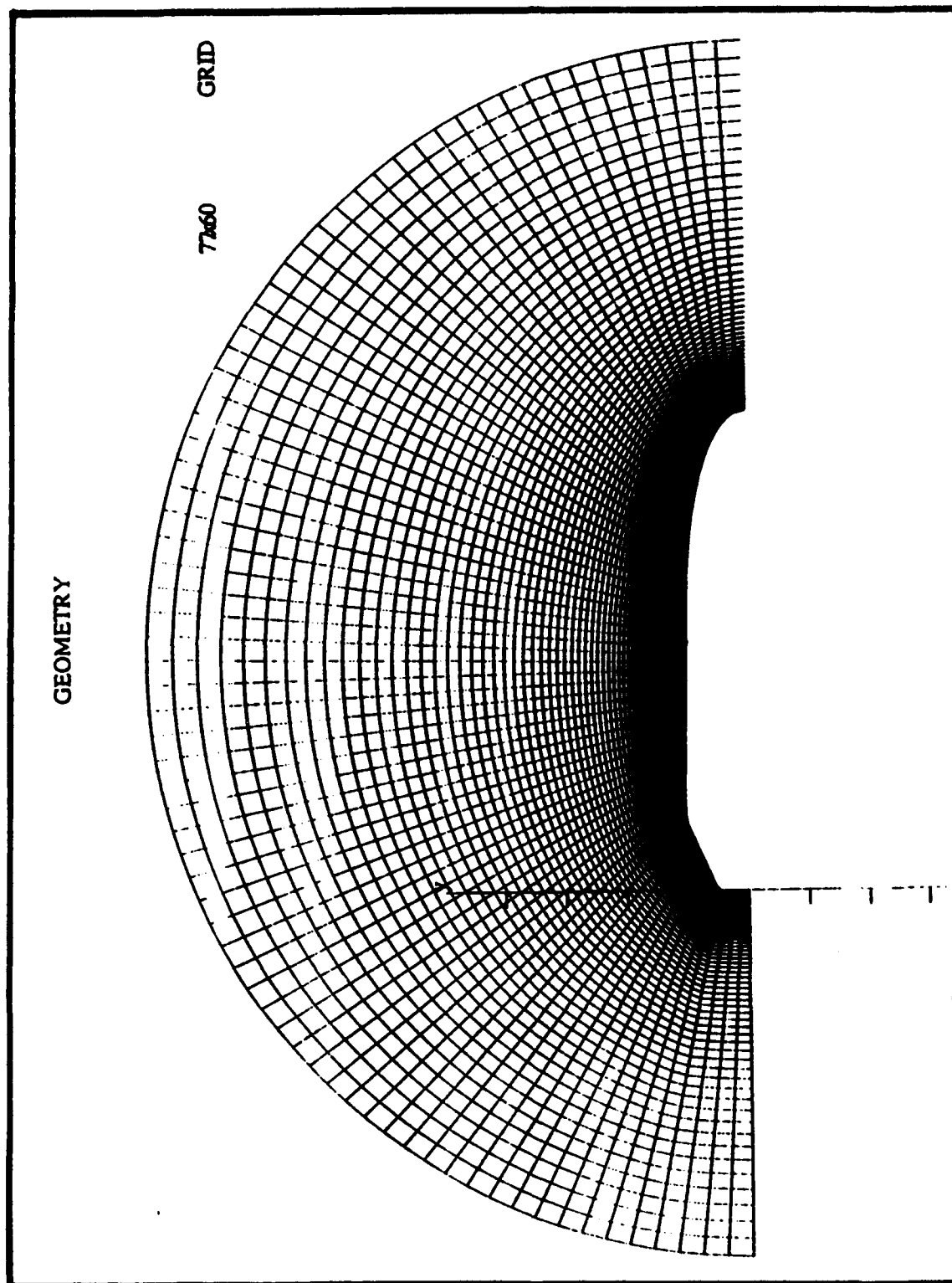Figure 11. 2D grid, complete body with conical afterbody.

51
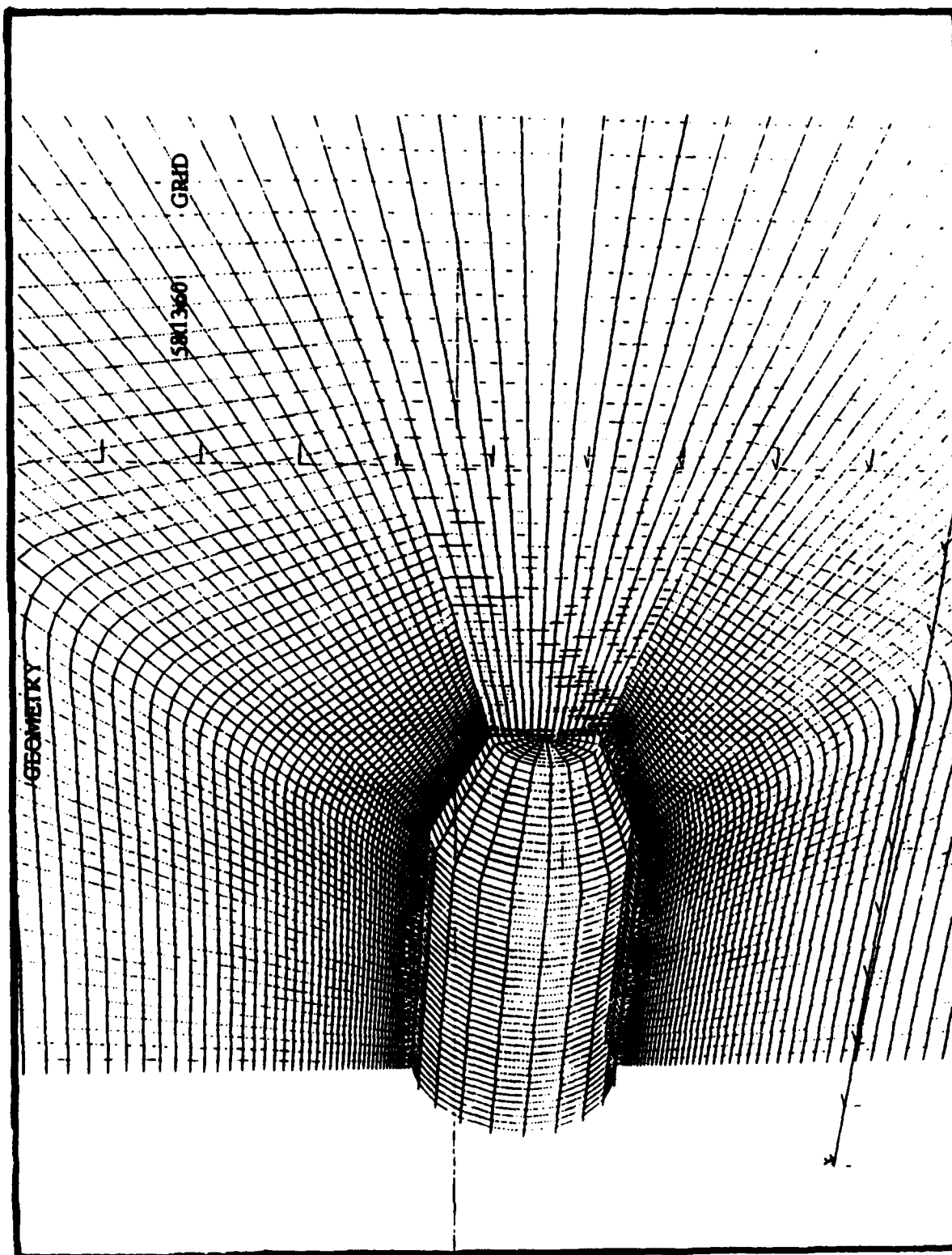
Figure 12. 3D grid, conical afterbody model.
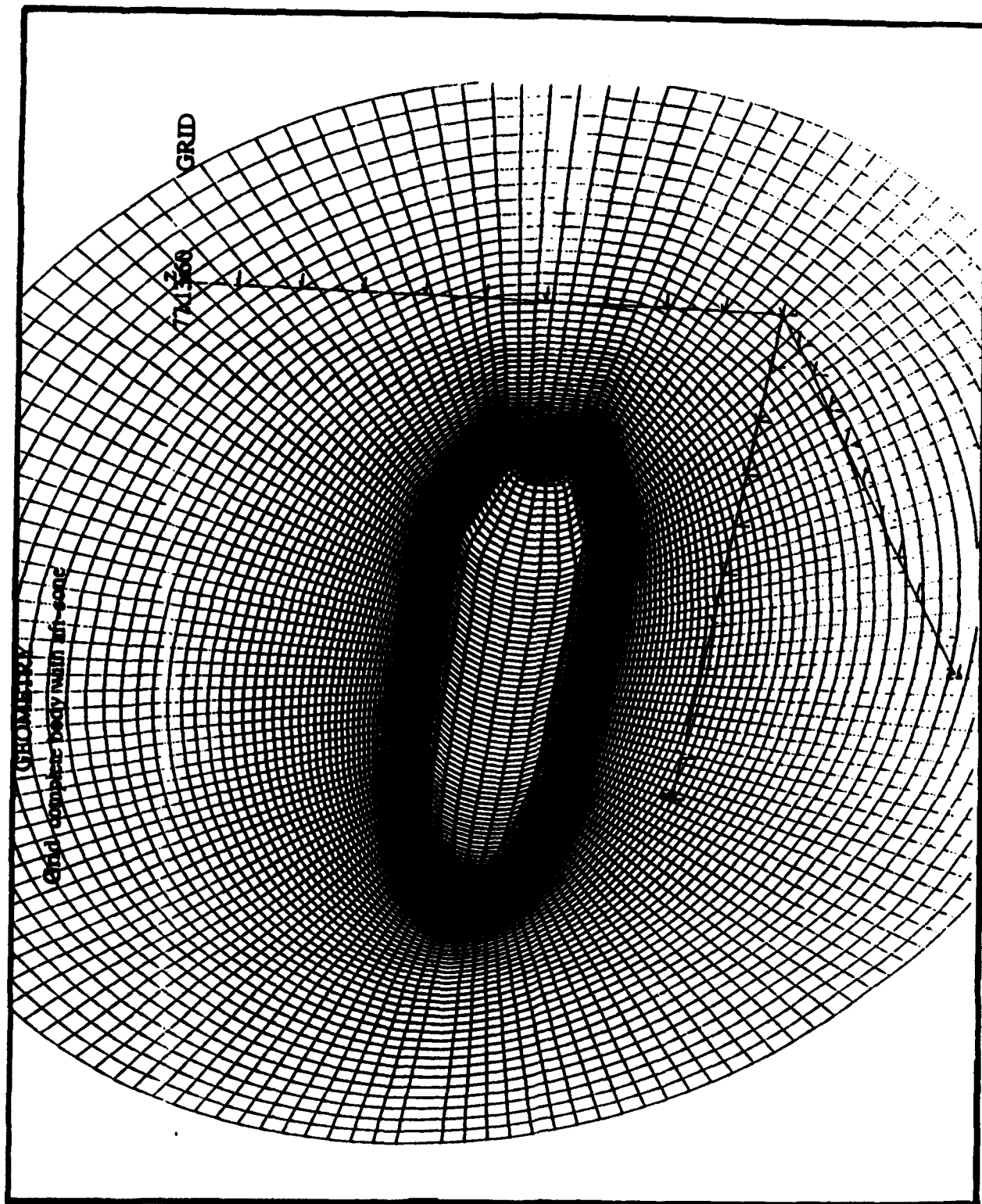
Figure 13. 3D grid, complete body with conical afterbody.
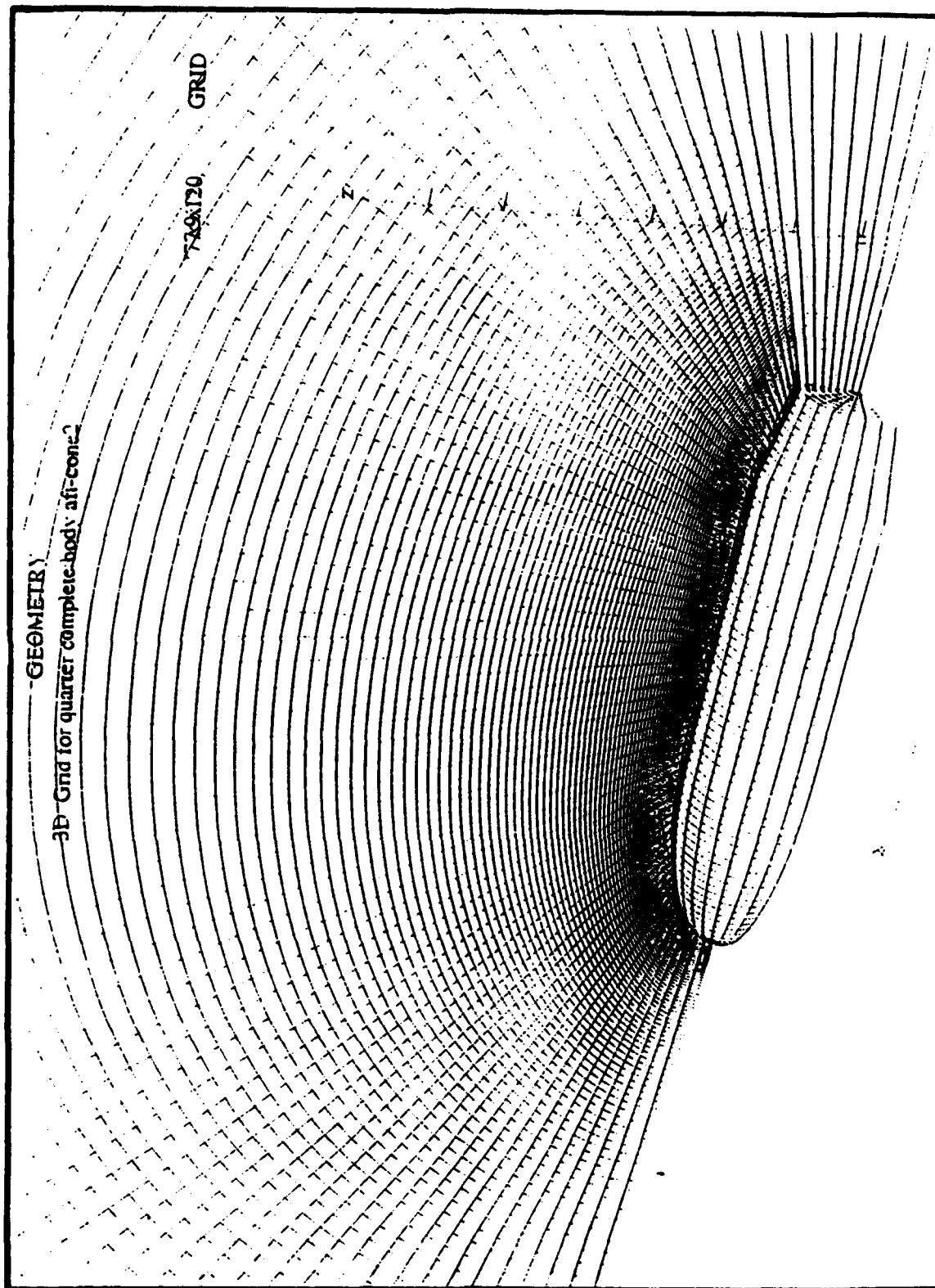
Figure 14. 3D fine-grid, complete body with conical afterbody.
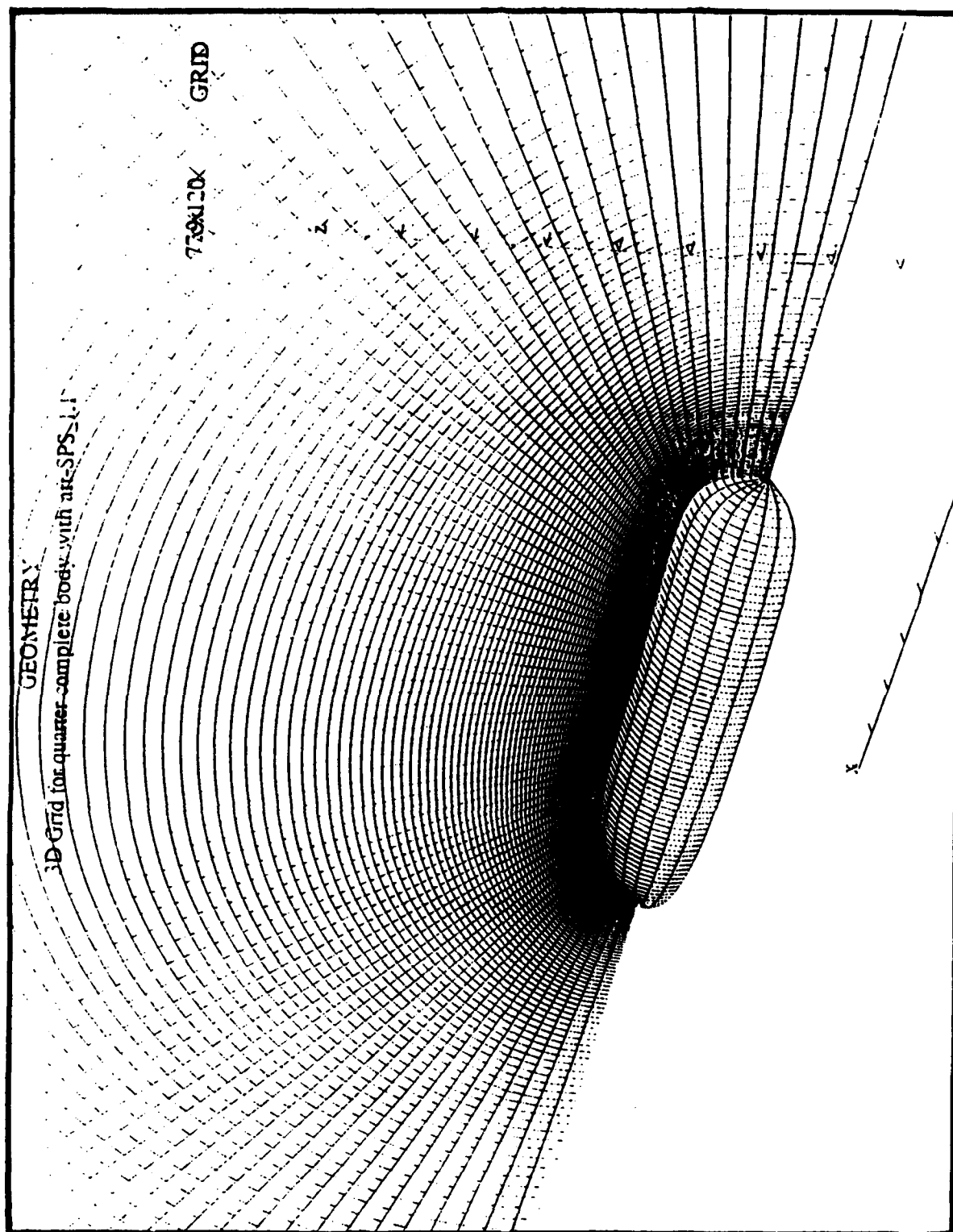
Figure 15. 3D fine-grid, complete body with SPS_1.1.
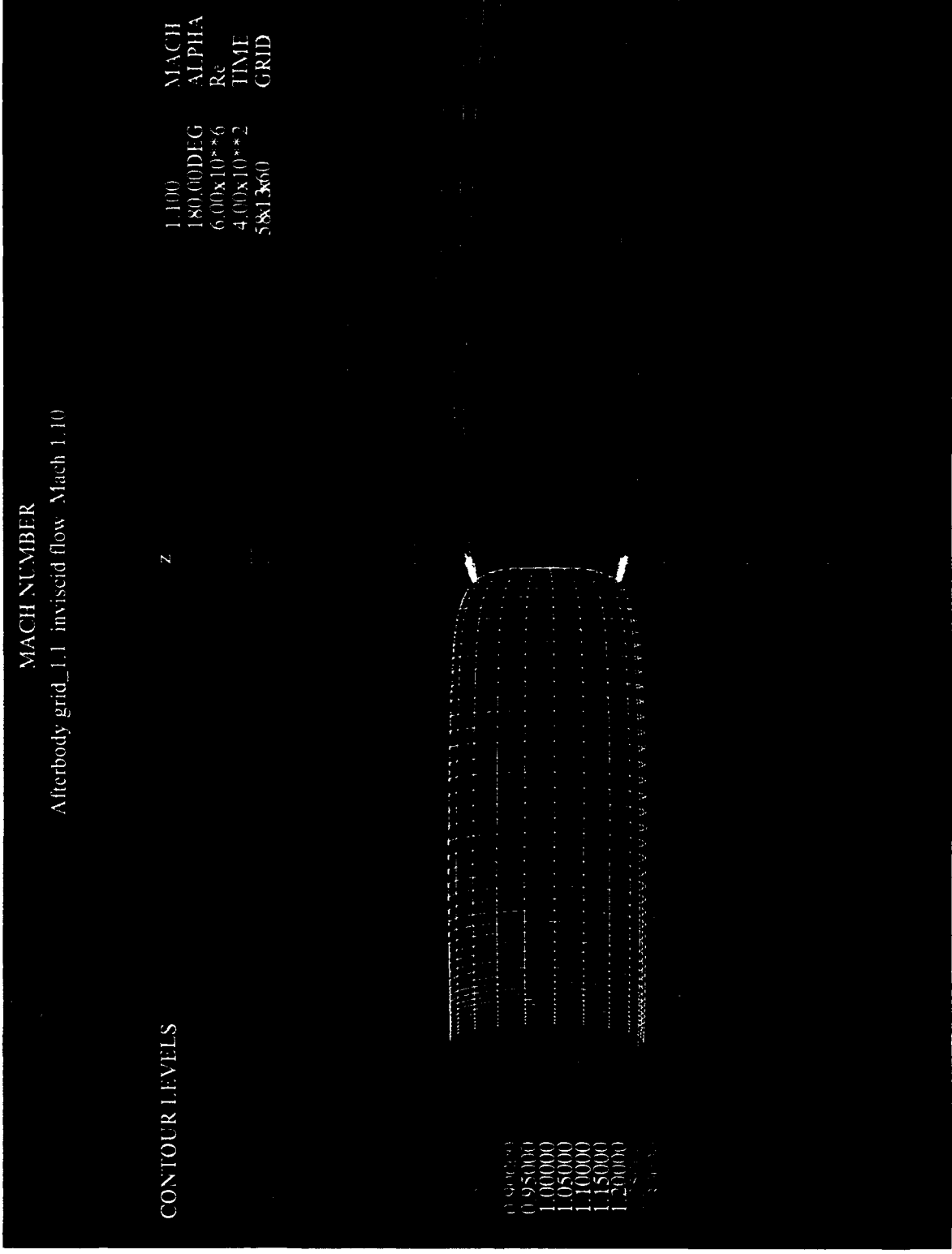
Figure 16. Afterbody model SPS_1.1, inviscid flow, Mach 1.10.

MACH NUMBER
Grid_1.1 inviscid flow Mach=1.20

MACH	1.200
ALPHA	180.00DEG
Re	6.00x10**6
TIME	4.00x10**2
GRID	58x13x60

CONTOUR LEVELS
0.00000
0.05000
0.10000
0.15000
0.20000
0.25000
0.30000
0.35000
0.40000
0.45000
0.50000
0.55000
0.60000
0.65000
0.70000
0.75000

1.50000
1.55000
1.60000
1.65000
1.70000
1.75000
1.80000
1.85000

z
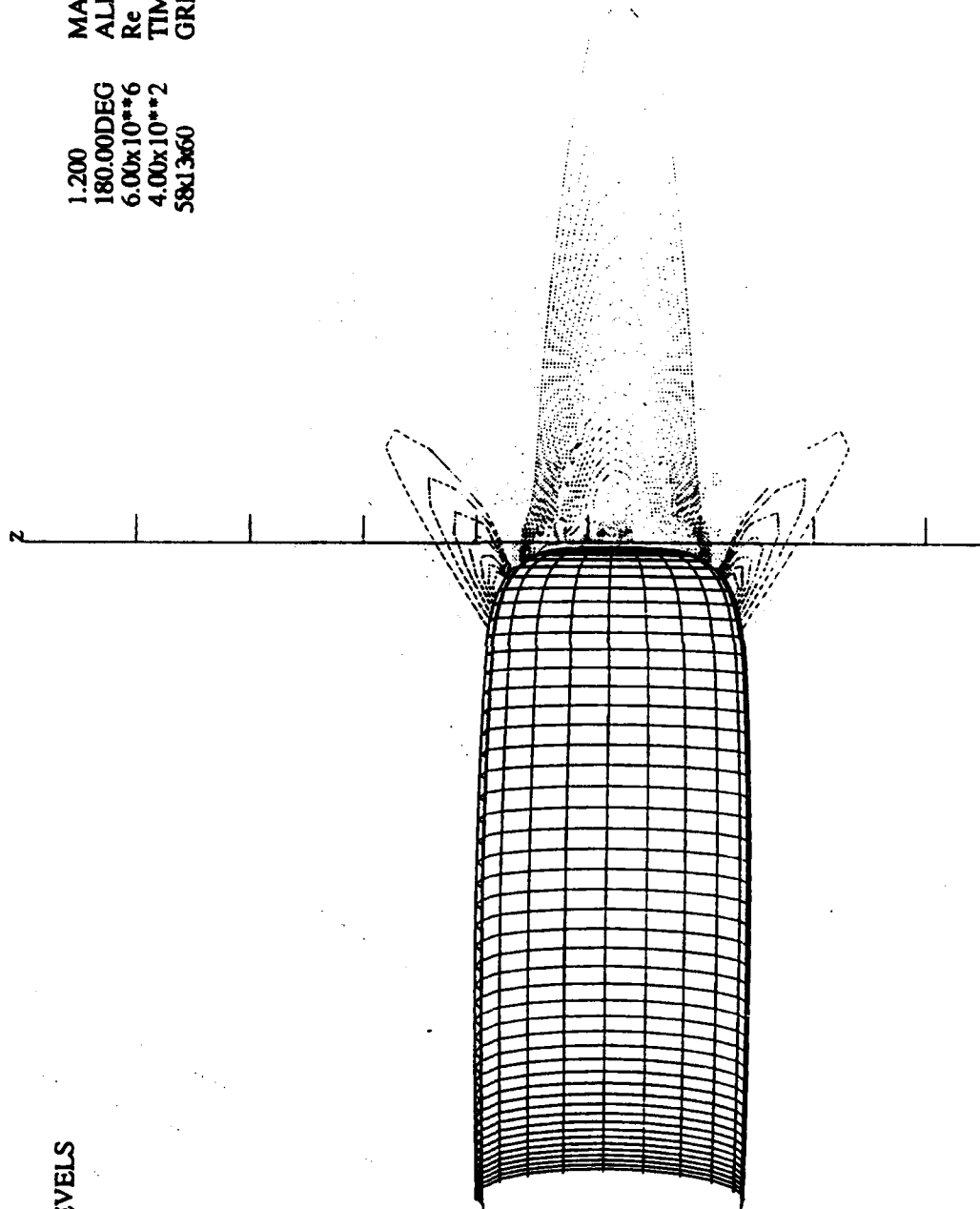
Figure 17. Afterbody model SPS_1.1, inviscid flow, Mach 1.20 .

57
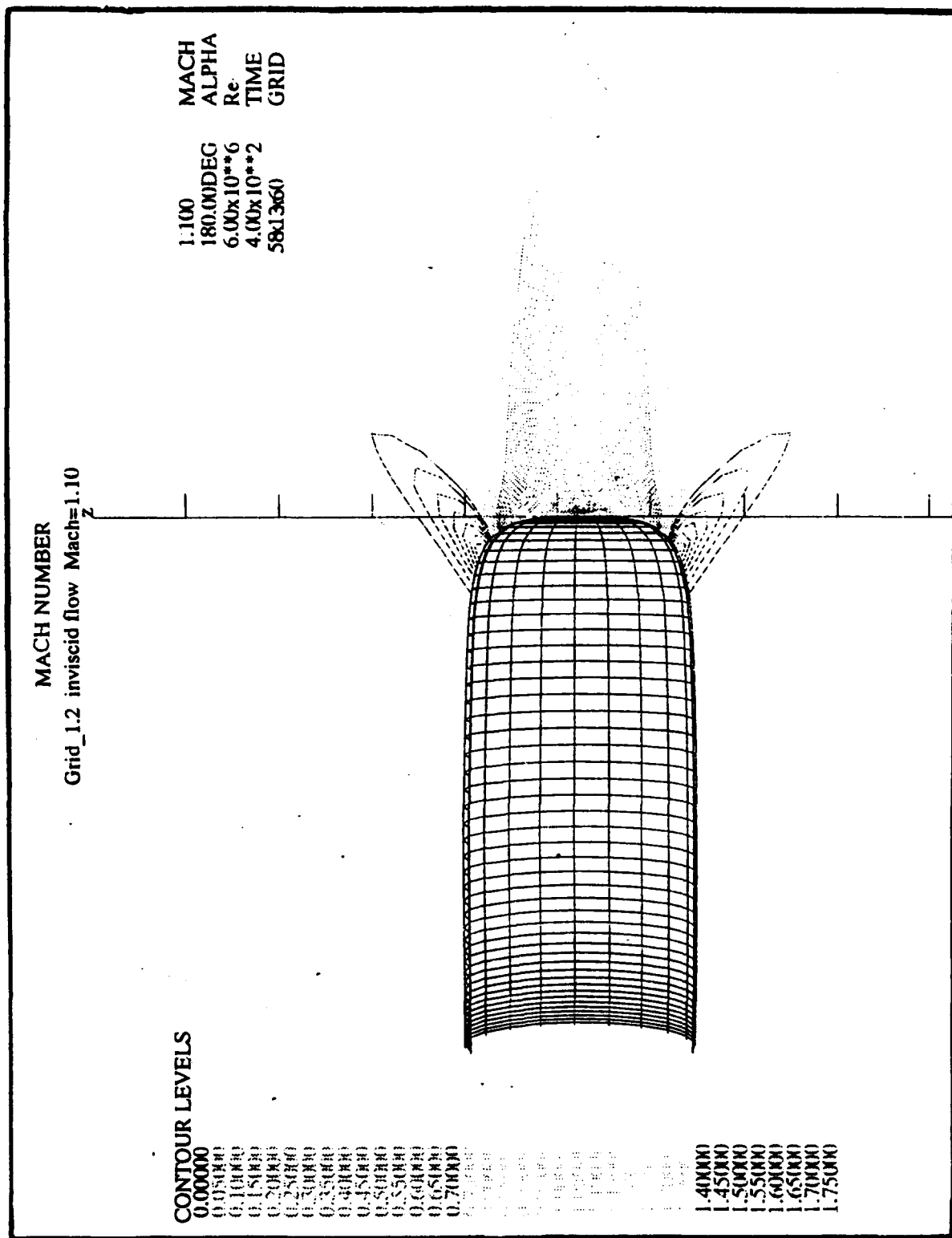
Figure 18. Afterbody model SPS_1.2, inviscid flow, Mach 1.10.

Figure 19. Afterbody model **SPS_1.2**, inviscid flow , Mach 1.20 .

MACH NUMBER
Grid_1.0 inviscid flow Mach=1.10

CONTOUR LEVELS
0.00000
0.05000
0.10000
0.15000
0.20000
0.25000
0.30000
0.35000
0.40000
0.45000
0.50000
0.55000
0.60000
0.65000
0.70000

1.45000
1.50000
1.55000
1.60000
1.65000
1.70000
1.75000
1.80000

MACH   1.100
ALPHA   180.00DEG
Re   6.00x10**6
TIME   4.00x10**2
GRID   5x13x60
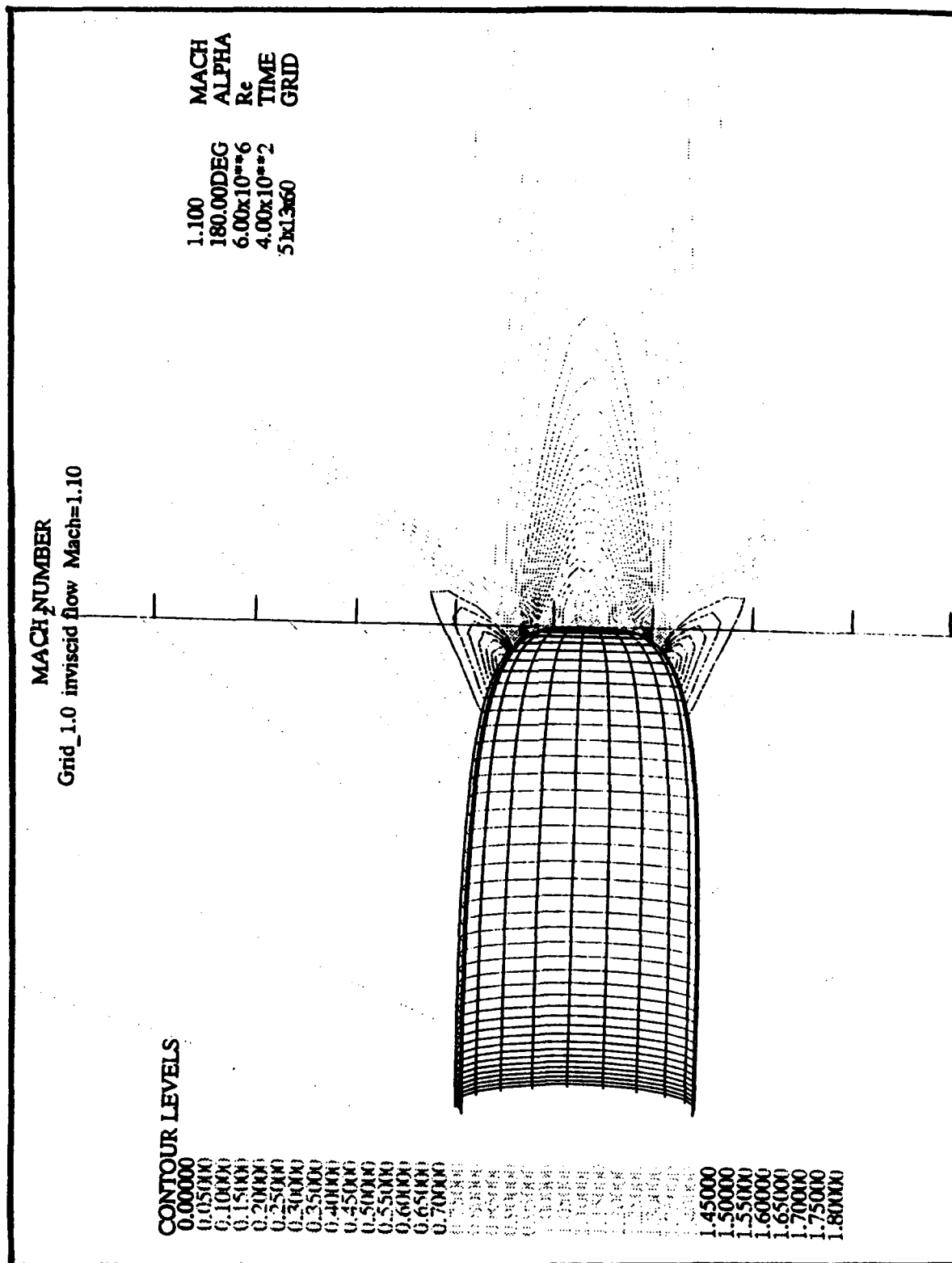
Figure 20. Afterbody model SPS_1.0, inviscid flow, Mach 1.10.

60
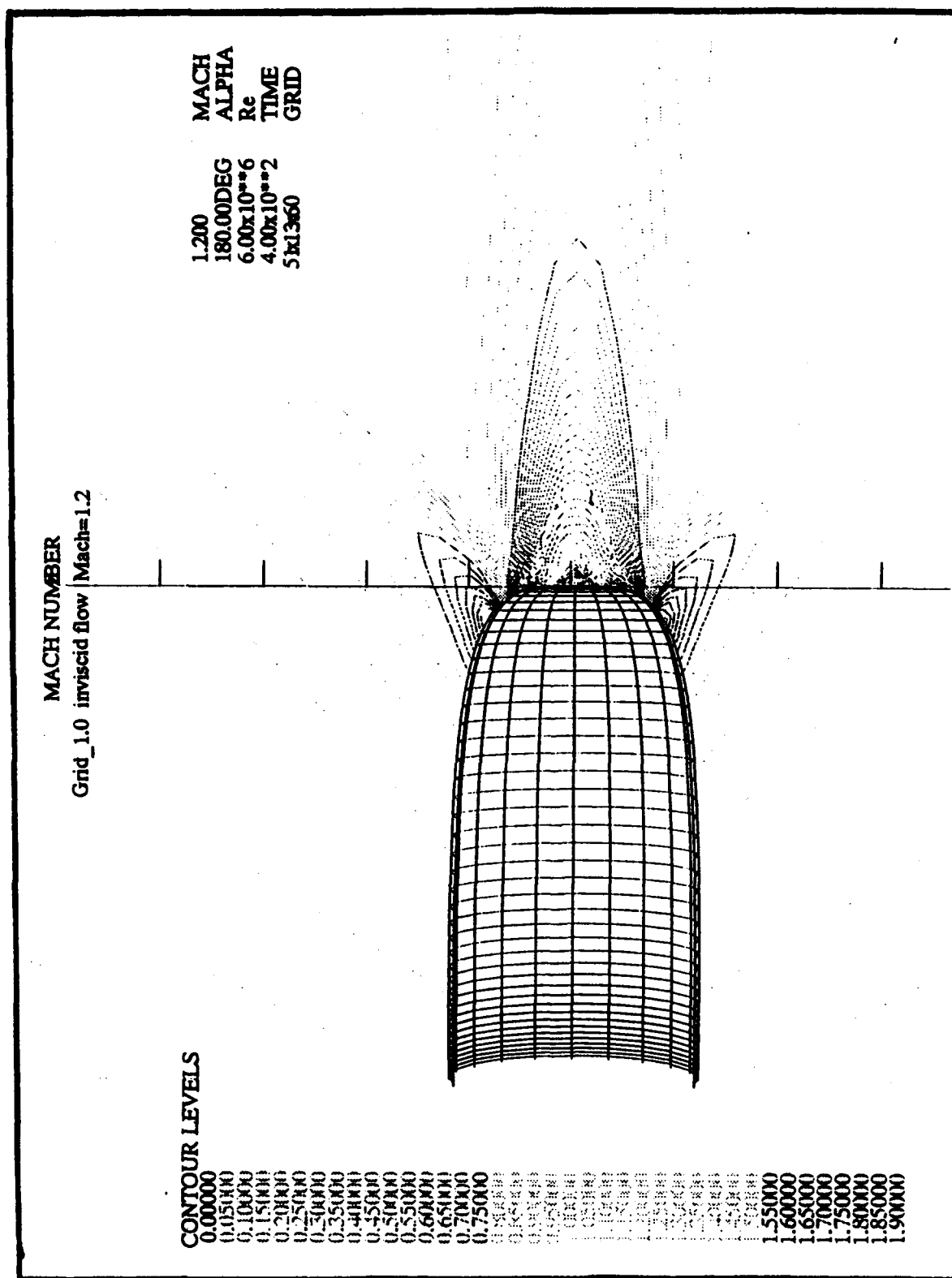
Figure 21. Afterbody model SPS_1.0, inviscid flow, Mach 1.20.
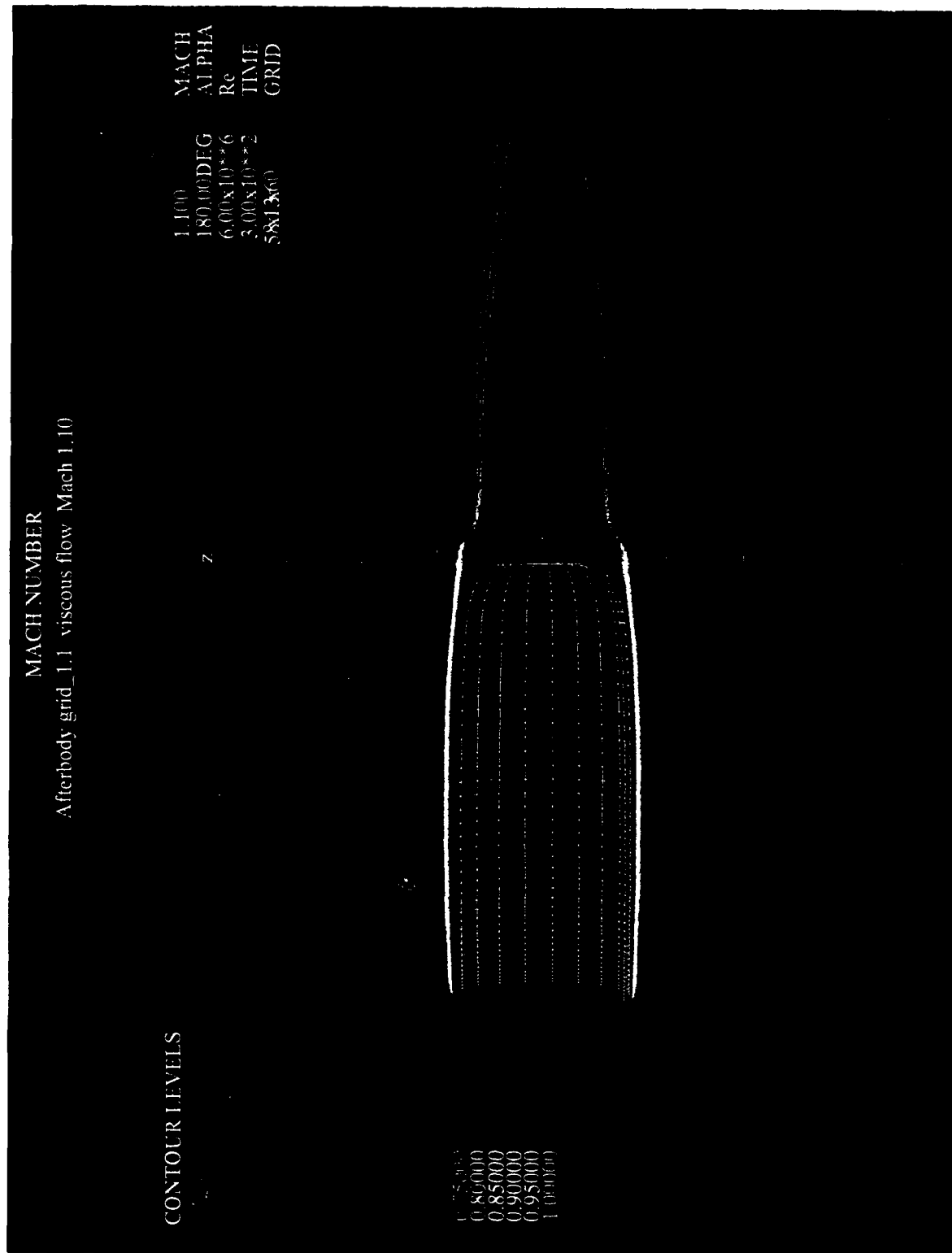
Figure 22. Afterbody model SPS_1.1, viscous flow, Mach 1.10.
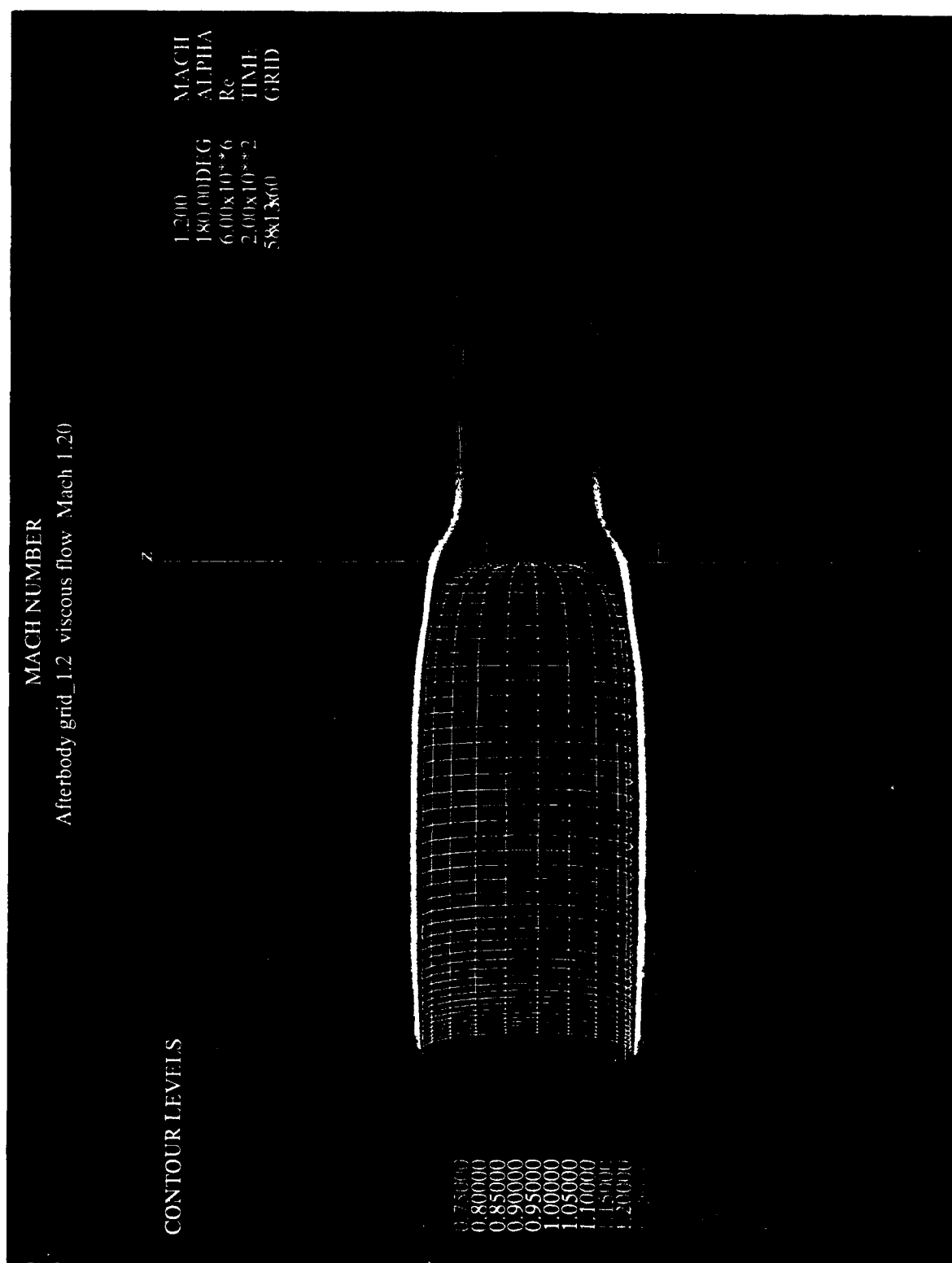
Figure 23. Afterbody model SPS_1.2 , viscous flow , Mach 1.20 .

MACH NUMBER
Aft-cone inviscid flow Mach 1.10

MACH   1.100
ALPHA   180.00DEG
Re   6.00x10**6
TIME   3.00x10**2
GRID   58x13x60

CONTOUR LEVELS
0.00000
0.05000
0.10000
0.15000
0.20000
0.25000
0.30000
0.35000
0.40000
0.45000
0.50000
0.55000
0.60000
0.65000
0.70000
0.75000

1.50000
1.55000
1.60000
1.65000
1.70000
1.75000
1.80000
1.85000
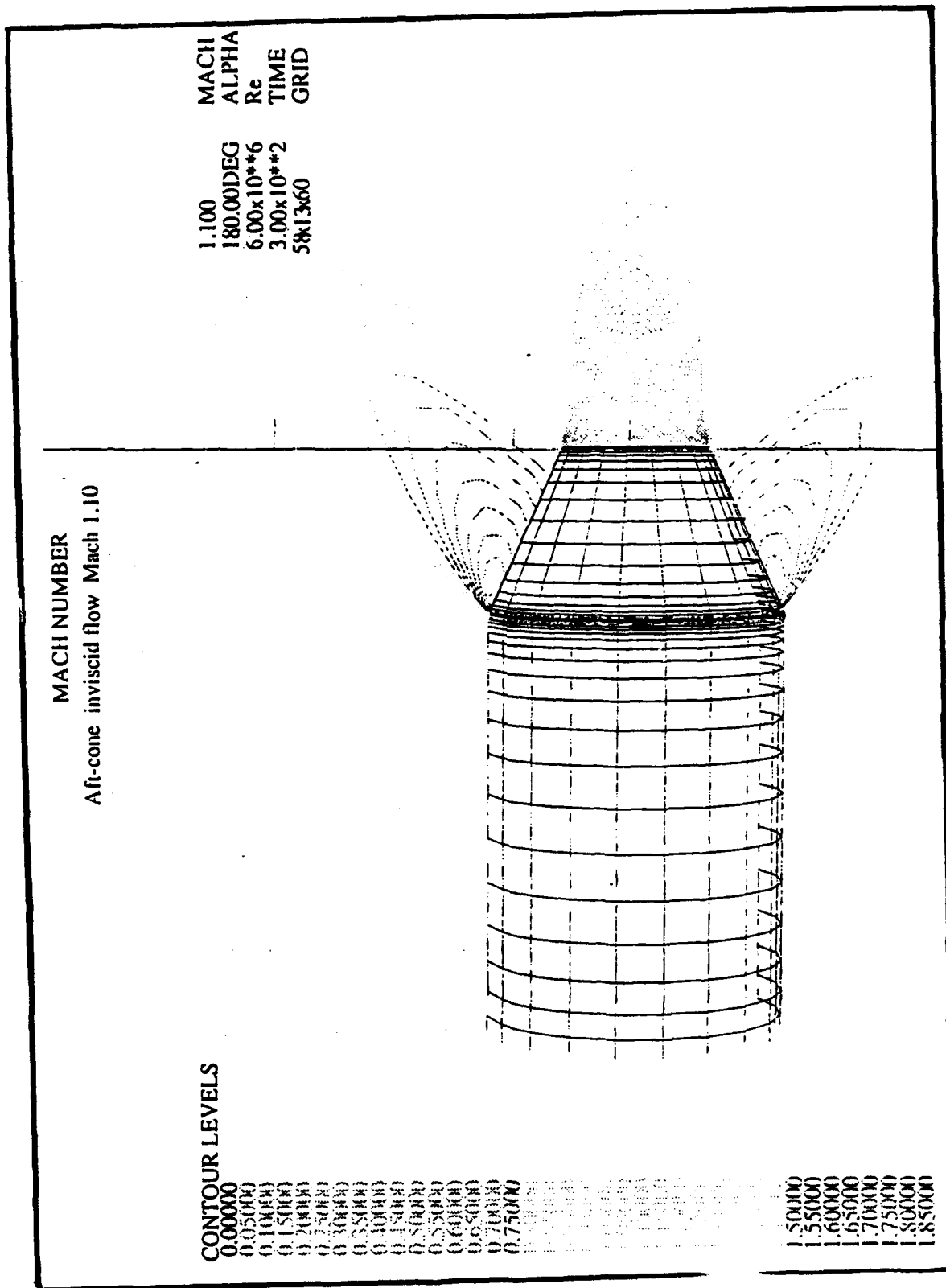
Figure 24. Conical afterbody model, inviscid flow, Mach 1.10.

MACH NUMBER
Aft-cone viscous flow Mach 1.10

MACH	1.100
ALPHA	180.00DEG
Re	6.00x10**6
TIME	3.00x10**2
GRID	58x13x60

CONTOUR LEVELS
0.00000
0.05000
0.10000
0.15000
0.20000
0.25000
0.30000
0.35000
0.40000
0.45000
0.50000
0.55000
0.60000
0.65000

1.30000
1.35000
1.40000
1.45000
1.50000
1.55000
1.60000
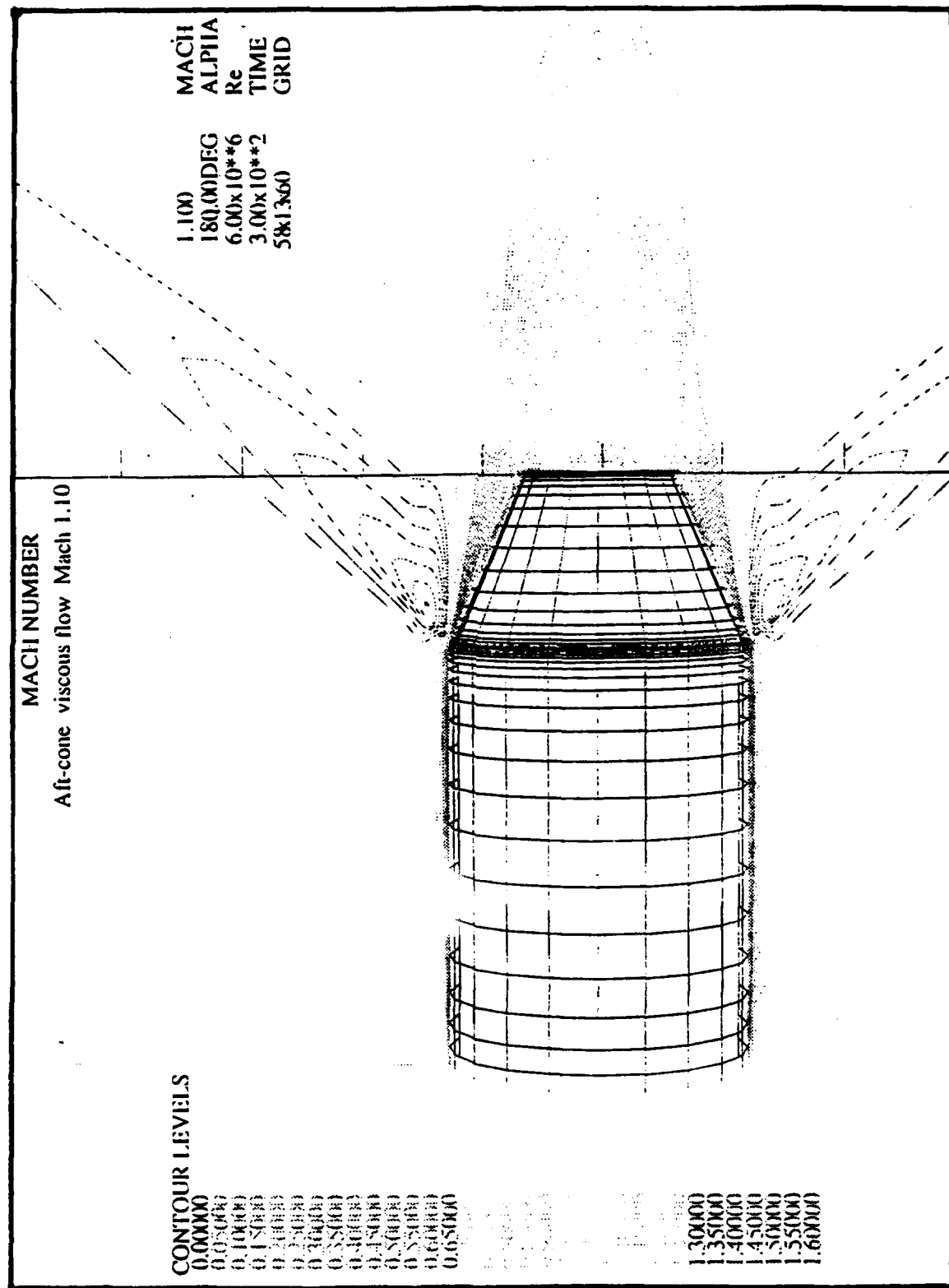
Figure 25. Conical afterbody model, viscous flow, Mach 1.10.
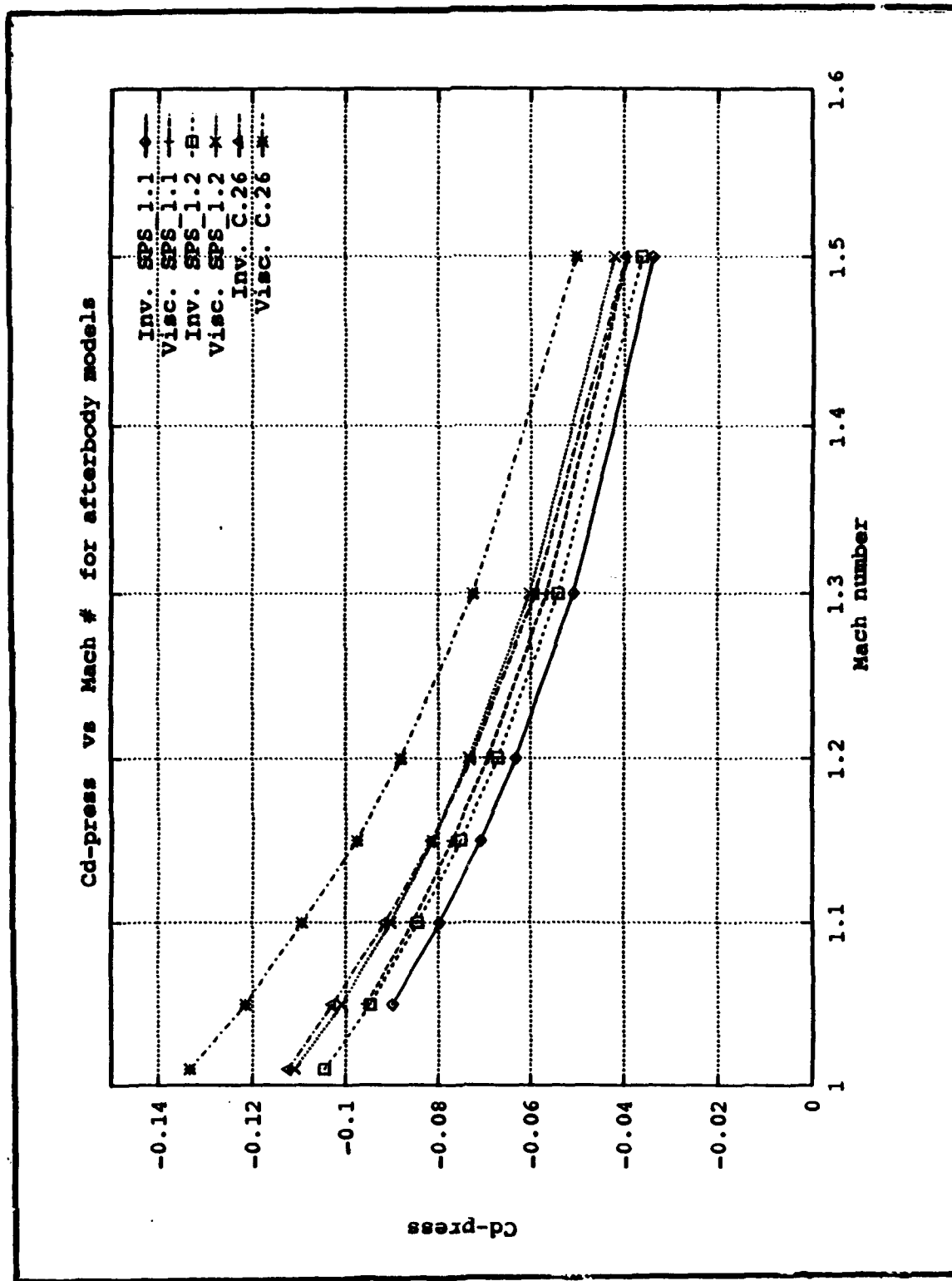
Figure 26. C_d - press. versus Mach number for afterbody models.
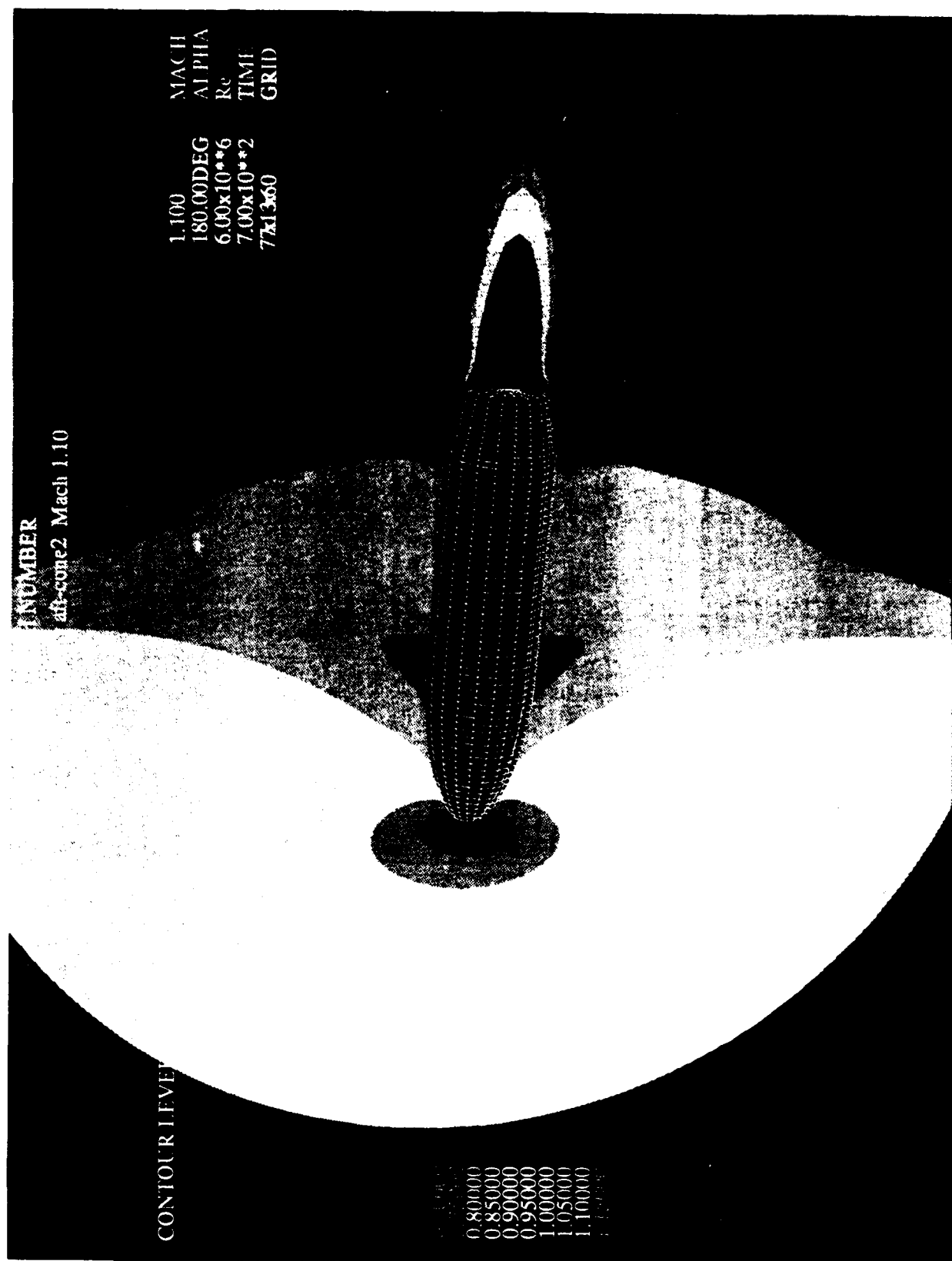
Figure 27. Coarse-grid (77x13x60) for half complete body models.

MACH NUMBER
Quarter complete body aft-cone2 Mach 1.10

MACH	1.100
ALPHA	180.00DEG
Re	6.00x10**6
TIME	6.00x10**2
GRID	77x9x120

CONTOUR LEVELS
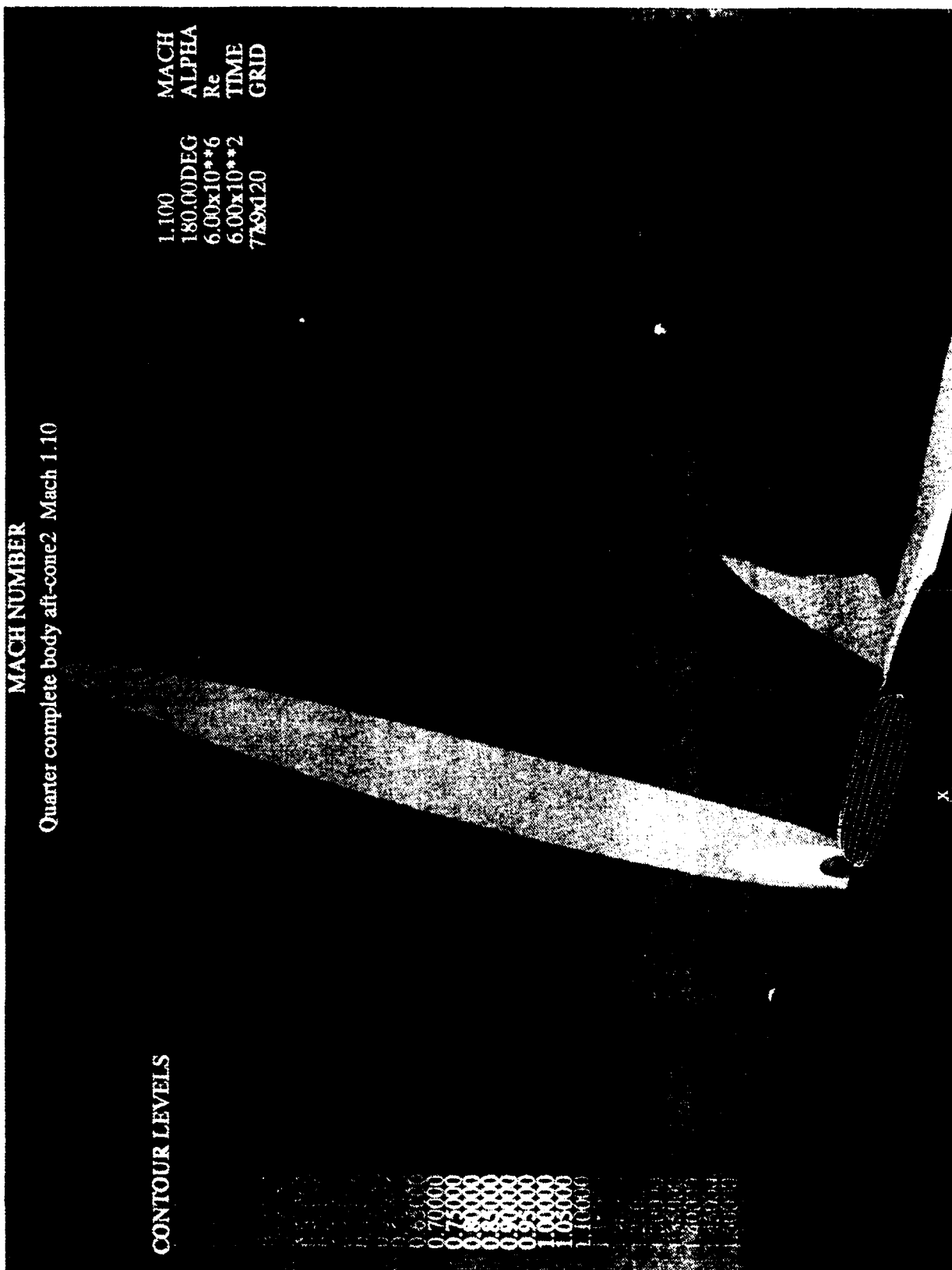
Figure 28. Fine-grid (77x9x120) for quarter complete body models.
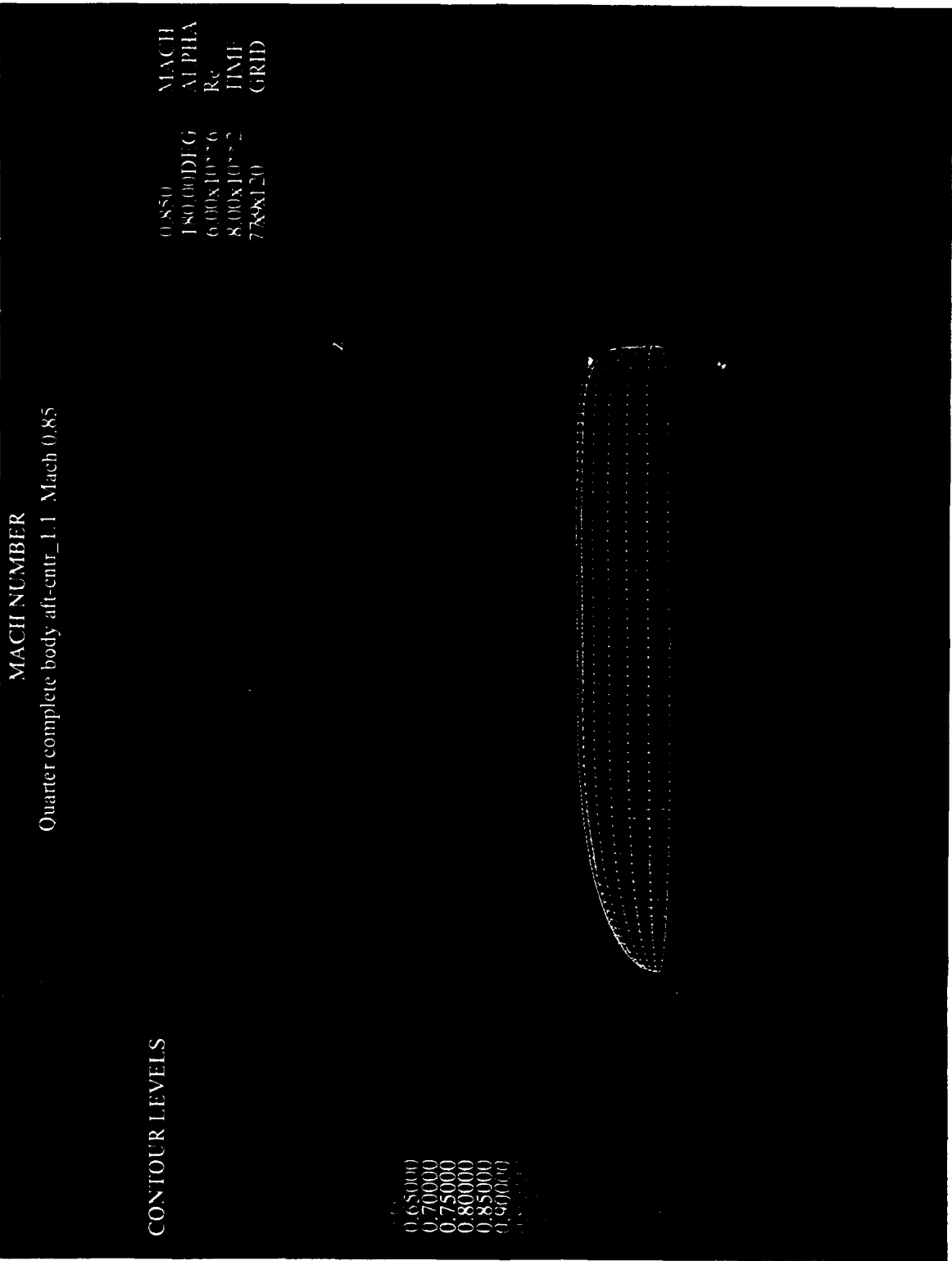
Figure 29. Quarter complete body aft-SPS_1.1, Mach 0.85 .
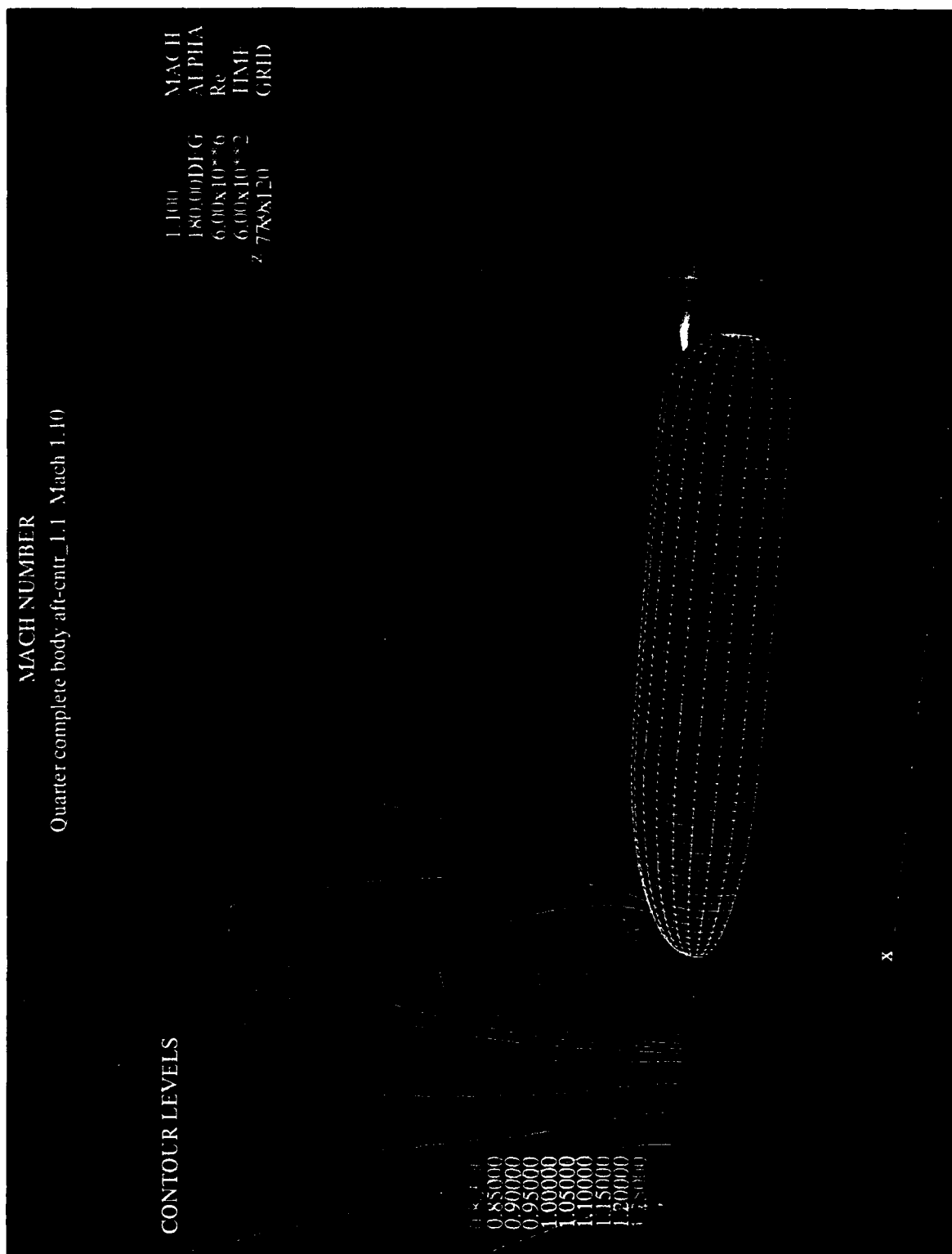
Figure 30. Quarter complete body aft-SPS_1.1 , Mach 1.10 .

MACH NUMBER

Quarter complete body aft-cntr_1.2   Mach 1.10

CONTOUR LEVELS

0.85000
0.90000
0.95000
1.00000
1.05000
1.10000
1.15000
1.20000
1.25000

MACH   1.100
ALPHA   180.00DEG
Re   6.00x10**6
TIME   6.00x10**2
GRID   78x8x120
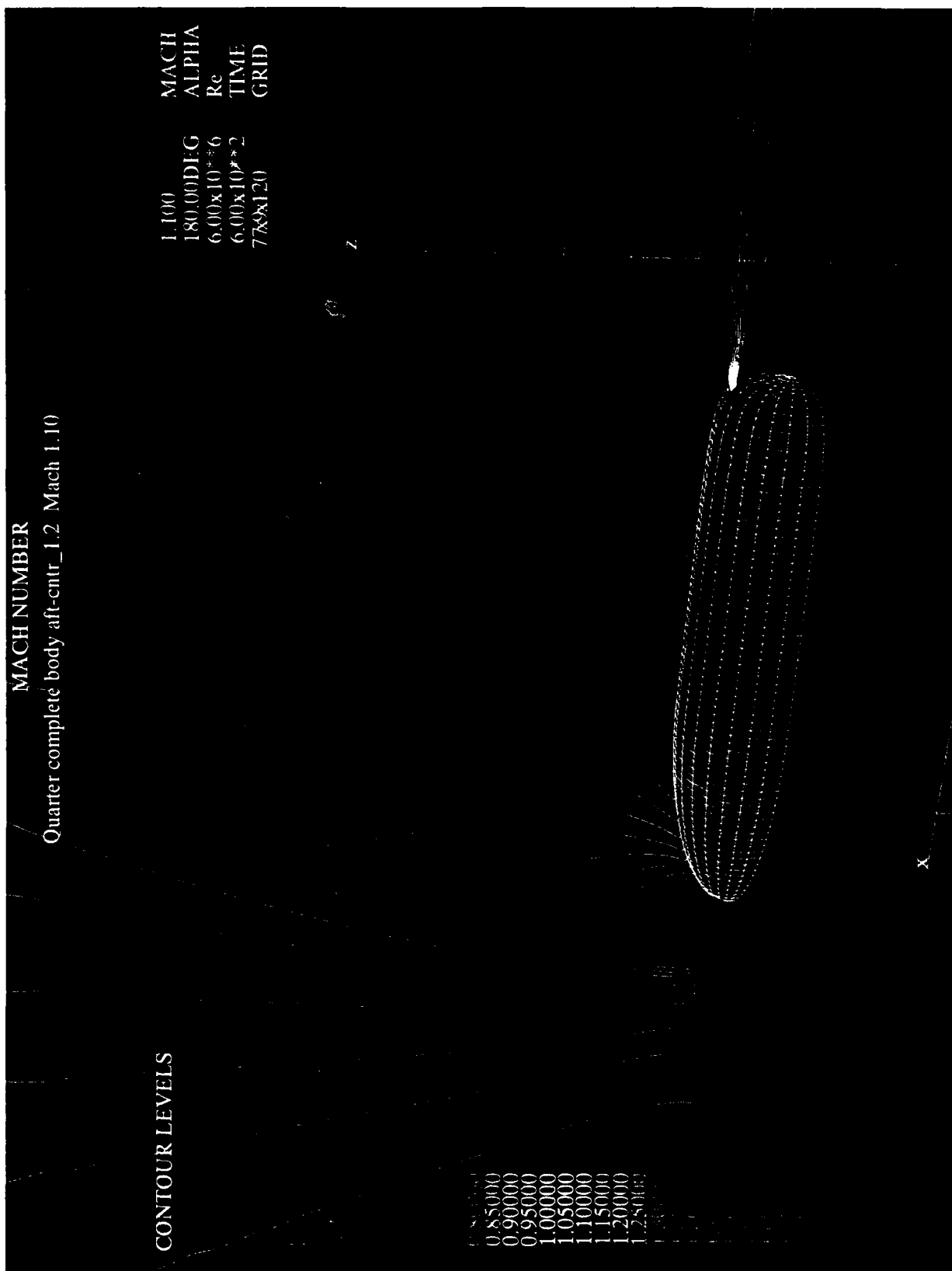
Figure 31. Quarter complete body aft-SPS_1.2 , Mach 1.20 .

Figure 32. Quarter complete body aft-SPS_1.1 , Mach 1.20 .
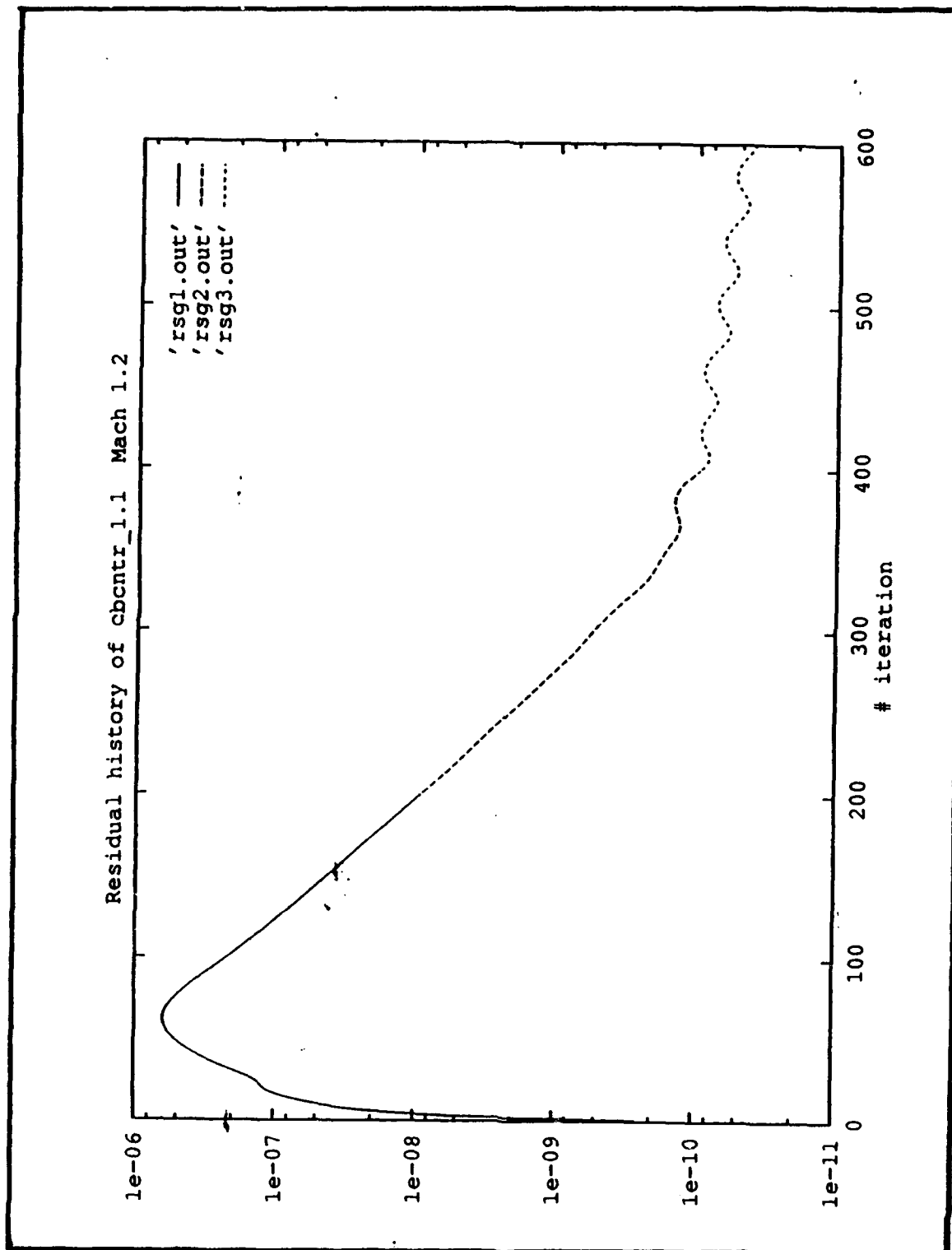
Figure 33. Residual history of complete body SPS_1.1, Mach 1.10.

73

MACH NUMBER

Quarter Complete body aft-cone2   Mach 1.10

MACH	1.100
ALPHA	180.00DEG
Re	6.00x10**6
TIME	6.00x10**2
GRID	77x9x120

CONTOUR LEVELS

0.75000
0.80000
0.85000
0.90000
0.95000
1.00000
1.05000
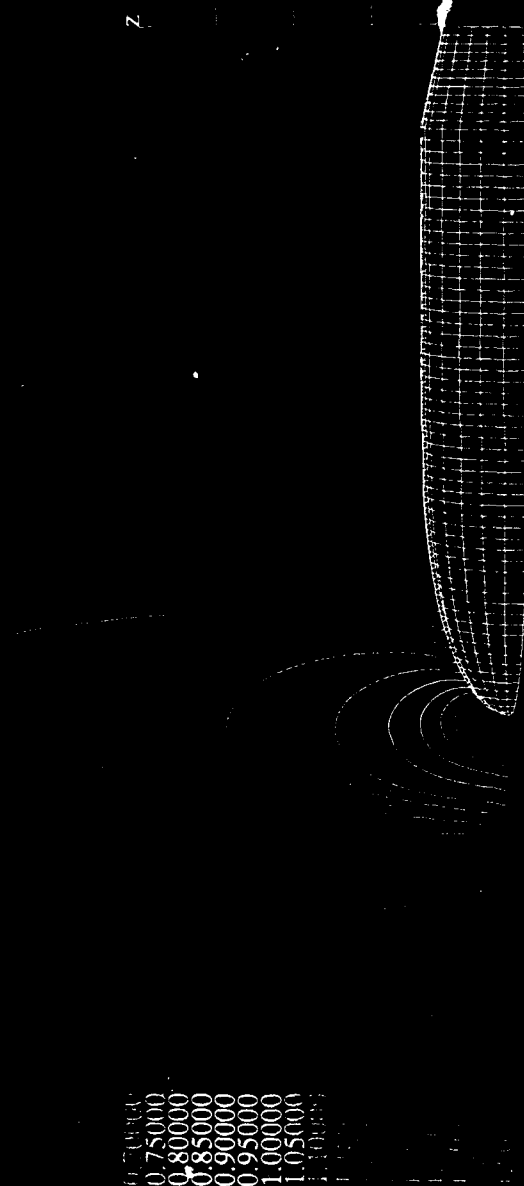
Figure 34. Quarter complete body aft-conical , Mach 1.10 .
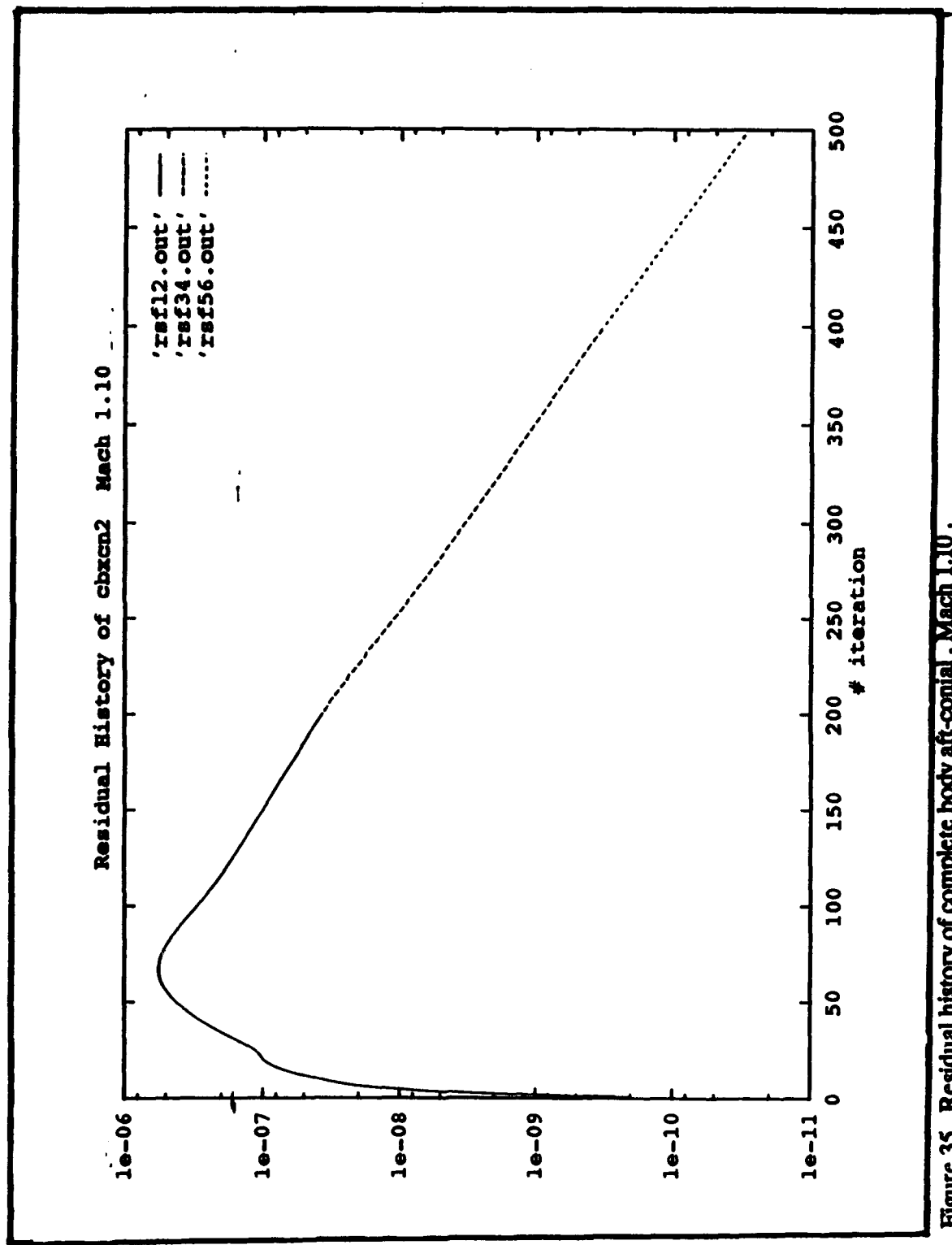
Figure 35. Residual history of complete body aft-conial, Mach 1.10.
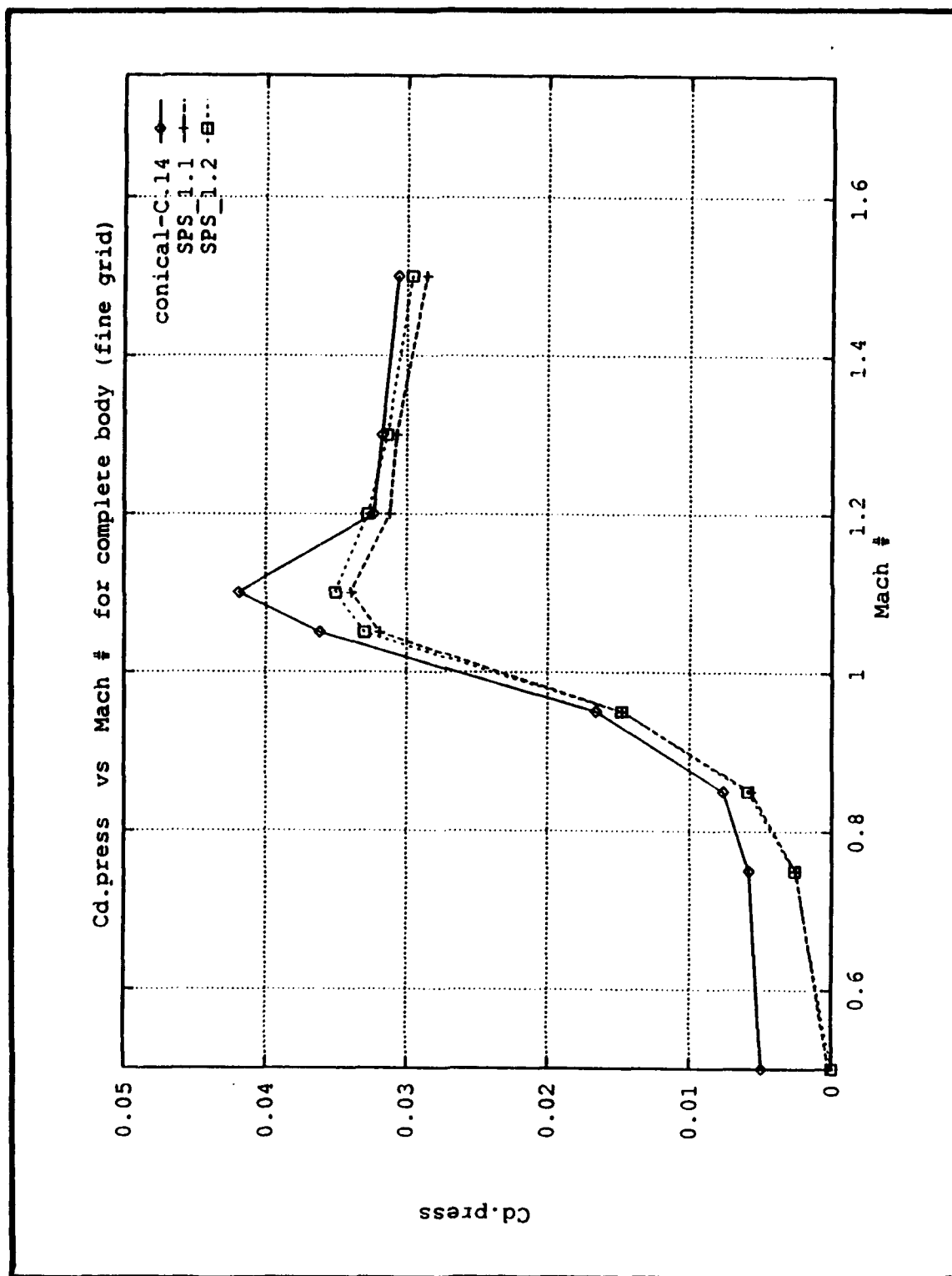
Figure 36. C_d - press. versus Mach number for quarter complete body models.

APPENDIX

COMPUTER PROGRAMS

```
      PROGRAM KSI.F
      ***********************************************************
      * This program is developed to calculate KSI(X), K(X) and X *
      *  using mumerical integration based on trapezoidal rule to *
      *  solve equation (32) and plotting the output as shown in  *
      *  Figs. 1 .                                                *
      ***********************************************************

            REAL M(3), X(0:401,3), A, A1, B(401,3)
      #        , KSI, P, FUNC, H, DD, Q, L, K(401,3), N, N1
            INTEGER YY
            OPEN(UNIT=9,FILE='KSI',STATUS='UNKNOWN')
            PRINT *,'ENTER LOWER & UPPER BOUND, # OF INTERVALS, # OF
      #DATA SET'
            READ *, A, A1, N, N1
      100   DO 10 I=1,3
            PRINT*, 'ENTER MACH NO.'
            READ*, M(I)
      C           M(I) = 0.9+I*0.1
            IF (M(I).LT.1.0) THEN
            P = -1.
            ELSE
            P = 1.
            ENDIF
            DO 20 J=1,N1
                B(J,I) = J*A1/N1
                H = (B(J,I)-A)/N
                AREA = 0.
                K(J,I)=(-0.0102/(M(I)**2))*((ABS((B(J,I)**2)-((ABS(1-
      #  M(I)**2))**1.7574)))**(2./3.)+(ABS(1-M(I)**2))**1.1716)
      C
                DO 30 L= 1,N
                    KSI = A + (L-0.5)*H
                    DD = (KSI**2+P*(ABS(1-M(I)**2))**1.7574)
                    IF (DD.GT.0.0) THEN
                    FUNC = 1./(DD**(1./3.))
                    Q = 1.
                    ELSE
                    FUNC = 1./((-1.*DD)**(1./3.))
                    Q = -1.
                    ENDIF
                    AREA = AREA + H*FUNC*Q
                    X(J,I) = AREA
      30        CONTINUE
      20        CONTINUE
      10        CONTINUE
      C
            DO 40 J= 1,N1
                PRINT 50, (B(J,I),X(J,I),K(J,I),I=1,3)
```

78

```fortran
50         FORMAT(1X,3(F6.3,2F10.5,1X))
40    CONTINUE
C
 200  PRINT*,'TRY AGAIN?, ENTER 1 FOR YES,2 FOR DATA FILE,
     # OTHERS FOR NO'
      READ*, YY
      IF (YY.EQ.1) THEN
        GO TO 100
      ELSE
          IF (YY.EQ.2) THEN
              DO 110 J= 1,N1
              WRITE (9,50) (B(J,I),X(J,I),K(J,I),I=1,3)
 110          CONTINUE
              GO TO 200
          ENDIF
      ENDIF
      END




PROGRAM ZETA.F
***********************************************************
*  This program is written to calculate ZETA(r) and r using*
*  equation (29) and plotting output in Fig.3 .           *
***********************************************************

      REAL M(3), ZETA(0:14,3), R(14)
      OPEN(UNIT=9,FILE='ZZ',STATUS='UNKNOWN')
C
      DO 10 I= 1,3
C        M(I) = 0.7+I*0.1
         PRINT*, 'ENTER MACH NO.'
         READ*, M(I)
         DO 20 J= 1,14
         ZETA(0,I) = 1000.0
         PRINT*, 'ENTER R VALUES'
         READ*, R(J)
C        R(J) = 0.1*J
         ZETA(J,I) = (4/(R(J)**2))+(ABS(1-(M(I)**2))
     #   *(R(J)**2.8284))
     #   +((1-M(I)**2)*(R(J)**7.657)/50.63
         IF (ZETA(J,I).GE.ZETA(J-1,I) ZETA(J,I)=ZETA(J-1,I)
 20      CONTINUE
 10   CONTINUE
C
      PRINT 30, M
 30   FORMAT(11X,5F10.4)
      DO 40 J= 1,14
      WRITE(9,50) (R(J), (ZETA(J,I),I=1,4)
 50   FORMAT(4X,3'2F10.4,2X)
 40   CONTINUE
      END
```

```
PROGRAM D2D3.F
********************************************************************
*     This program will read data files output Gridgen2d    *
*     from 2D to 3D for further processing with rotategr.f  *
********************************************************************

      REAL X(77,60),Y(77,60),Z(77,60)
      READ(12,*)  IDIM,JDIM
      READ(12,*)  ((X(I,J),I=1,IDIM),J=1,JDIM),
     #            ((Y(I,J),I=1,IDIM),J=1,JDIM)
      Z(I,J)=0.0
      WRITE(14,*)  IDIM,JDIM,1
      WRITE(14,*)  ((X(I,J),I=1,IDIM),J=1,JDIM),
     #             ((0.0,I=1,IDIM),J=1,JDIM),
     #             ((Y(I,J),I=1,IDIM),J=1,JDIM)
      STOP
      END
```

```
PROGRAM HALF.F
********************************************************************
*     This program will write out half of a grid file output  *
*     from Grape for further processing with rotategr.f        *
********************************************************************

      DIMENSION X(200,200),Y(200,200)
      READ(30,*)  IDIM,JDIM
      READ(30,*)  ((X(I,J),I=1,IDIM),J=1,JDIM),
     #            ((Y(I,J),I=1,IDIM),J=1,JDIM)
C
      IDMD2=IDIM/2 + 1
C
      DO 10 J=1,JDIM
            Y(IDIM2,J) = 0.0
  10  CONTINUE
C
      WRITE(31,*)  IDMD2,JDIM,1
      WRITE(31,*)  ((X(I,J),I=IDMD2),J=1,JDIM),
     #             ((0.0,I=IDMD2),J=1,JDIM),
     #             ((Y(I,J),I=IDMD2),J=1,JDIM)
      STOP
      END
```

```
PROGRAM ROTATEGR.F
********************************************************************
*    This program will create 3D grid (body of revolution)    *
*    by rotating 3D plane grid for further processing with     *
*    Flow Solver                                               *
********************************************************************

      DIMENSION X(200,200), Y(200,200), Z(200,200)
      DIMENSION XX(200,100,200), YY(200,100,200),
     #ZZ(200,100,200)
      CHARACTER*30 FNI
      CHARACTER*30 FNO
C
      PRINT*, 'INPUT GRID'
      READ(*,21) FNI
      PRINT*, 'SG = 0, MG = 1', ',UNF=1, FORM=2'
      READ(*,*) IGRI
      PRINT*, 'IFORI = 1 UNF, IFORI = 2 FORM'
      READ(*,*) IFORI
  21  FORMAT(A)
      IF (IFORI.EQ.1) THEN
      REWIND 1
      OPEN (1,FILE=FNI,FORM='UNFORMATTED')
      IF (IGRI.EQ.1) READ (1) MGR
      READ (1) I1,J1,K1
      READ (1) ((X(I,J),I=1,I1),J=1,J1),
     #         ((Y(I,J),I=1,I1),J=1,J1),
     #         ((Z(I,J),I=1,I1),J=1,J1)
      CLOSE (1)
      ENDIF
      IF (IFORI.EQ.2) THEN
      REWIND 2
      OPEN (2,FILE=FNI,FORM='FORMATTED')
      IF (IGRI.EQ.1) READ(2,*) MGR
      READ(2,*) I1,J1,K1
      READ(2,*) ((X(I,J),I=1,I1),J=1,J1),
     #          ((Y(I,J),I=1,I1),J=1,J1),
     #          ((Z(I,J),I=1,I1),J=1,J1)
      CLOSE (2)
      ENDIF
C
      PI = 4.*ATAN(1.)
      PRINT*, 'NO OF PLANE IN J DIRECTION ?'
      READ(5,*) JM
      DTH = (180./(JM-1))*(PI/180)
      DO 11 I=1,I1
      DO 11 J=1,J1
      K=J
      XX(I,2,K) = X(I,K)
      YY(I,2,K) = 0.0
      ZZ(I,2,K) = Z(I,K)
  11  CONTINUE
```

```
c
      IM=I1
      KM=J1
      DO 20 J=3,JM+1
      DO 20 I=1,IM
      DO 20 K=1,KM
      XX(I,J,K)=X(I,K)
      TH = (J-1)*DTH
      YY(I,J,K) = SIN(TH)*Z(I,K)
      ZZ(I,J,K) = COS(TH)*Z(I,K)
  20  CONTINUE
c
      DO 30 I=1,IM
      DO 30 K=1,KM
      J=1
      XX(I,J,K) = XX(I,J+2,K)
      YY(I,J,K) =-YY(I,J+2,K)
      ZZ(I,J,K) = ZZ(I,J+2,K)
      J=JM+2
      XX(I,J,K) = XX(I,J-2,K)
      YY(I,J,K) =-YY(I,J-2,K)
      ZZ(I,J,K) = ZZ(I,J-2,K)
  30  CONTINUE
      JM=JM+2
c
      PRINT*, 'Output filename ='
      READ(5,21) FNO
c
      REWIND 3
      OPEN( 3, FILE=FNO, FORM='UNFORMATTED')
      WRITE(3) IM,JM,KM
      WRITE(3) (((X(I,J,K), I=1,IM),J=1,JM),K=1,KM),
     #         (((Y(I,J,K), I=1,IM),J=1,JM),K=1,KM),
     #         (((Z(I,J,K), I=1,IM),J=1,JM),K=1,KM)
      CLOSE (3)
      STOP
      END
```

```
PROGRAM READX.F
****************************************************************
*      This program will read 3D grid file and convert from   *
*      formatted into unformatted file (grid.for to grid.in)  *
*      for further processing with Overflow.                  *
****************************************************************

       DIMENSION X(77,13,60), Y(77,13,60), Z(77,13,60)
       OPEN(UNIT=12,FILE='GRID.FOR',STATUS='UNKNOWN')
       OPEN(UNIT=14,FILE='GRID.IN',STATUS='NEW',
      #FORM='UNFORMATTED')
       READ(12,*) IDIM,JDIM,KDIM
       READ(12,20) (((X(I,J,K), I=1,IDIM),J=1,JDIM),K=1,KDIM),
      #            (((Y(I,J,K), I=1,IDIM),J=1,JDIM),K=1,KDIM),
      #            (((Z(I,J,K), I=1,IDIM),J=1,JDIM),K=1,KDIM)
C
       WRITE(14) IDIM,JDIM,KDIM
       WRITE(14) (((X(I,J,K), I=1,IDIM),J=1,JDIM),K=1,KDIM),
      #          (((Y(I,J,K), I=1,IDIM),J=1,JDIM),K=1,KDIM),
      #          (((Z(I,J,K), I=1,IDIM),J=1,JDIM),K=1,KDIM)
 20    FORMAT(6F15.6)
       STOP
       END




PROGRAM READQ.F
****************************************************************
*      This program will read q.save file output from         *
*      Overflow and convert from unformatted into formatted   *
*      file for further processing with Plot3d.               *
****************************************************************

       DIMENSION Q(77,13,60,5)
       OPEN(UNIT=1,FILE='Q.SAVE',STATUS='OLD',
      #FORM='UNFORMATTED')
       OPEN(20,FILE='Q.FORM',STATUS='NEW',FORM='FORMATTED' )
       READ(1) NI,NJ,NK
       READ(1) FSMACH,ALPHA,RE,TIME
       READ(1) ((((Q(I,J,K,NX) ,I=1,NI),J=1,NJ),K=1,NK),NX=1,5)
C
       WRITE(20,*) NI,NJ,NK
       WRITE(20,*) FSMACH,ALPHA,RE,TIME
       WRITE(20,*)((((Q(I,J,K,NX)

      #,I=1,NI),J=1,NJ),K=1,NK),NX=1,5)
       PRINT*, NI,NJ,NK
       STOP
       END
```

83

```
PROGRAM OVERFLOW.IN
*******************************************************************
*  Input file for Overflow to run either EULER or NAVIER-  *
*  STOKES Flow-solver.                                     *
*******************************************************************
  $GLOBAL
       CHIMRA=.F., NSTEP=100, RESTART=.F., NSAVE=100, NQT=0,
       $END
  $FLOINP
       ALPHA=180.0, FSMACH=0.95, REY= 6.00E6, TINF= 520.0,
       $END
  $GRDNAM
       NAME= 'AXI-SYMMETRIC BODY WITH AFT-CONE, 77x13x60
       GRID',
       $END
  $METPRM
       IRHS = 0, ILHS = 2, IDISS = 2,
       $END
  $TIMACU
       DT = 0.1, ITIME = 1, TFOSO = 1.00, CFLMIN = 5.00,
       $END
  $SMOACU
       ISPECJ = 2, DIS2J = 2.00, DIS4J = 0.02,
       ISPECK = 2, DIS2K = 2.00, DIS4K = 0.02,
       ISPECL = 2, DIS2L = 2.00, DIS4L = 0.02,
       SMOO = 1.00, EPSE = 0.35,
       $END
  $VISINP
       VISCJ = .F. , VISCK = .F. , VISCL = .F. ,
       NTURB =  0,
       ITTYP =  1,
       ITDIR =  3,
       JTLS  =  1,
       JTLE  = 77,
       KTLS  =  1,
       KTLE  = 13,
       LTLS  =  1,
       LTLE  = 60,
       TLPAR1=  .3,
       $END
  $BCINP
       NBC   = 6,
       IBTYP =    15,   12,   12,    1,   32,   15,
       IBDIR =     1,    2,   -2,    3,    3,   -1,
       JBCS  =     1,    1,    1,    1,    1,   77,
       JBCE  =     1,   77,   77,   77,   77,   77,
       KBCS  =     1,    1,   13,    1,    1,    1,
       KBCE  =    13,    1,   13,   13,   13,   13,
       LBCS  =     1,    1,    1,    1,   60,    1,
       LBCE  =    60,   60,   60,    1,   60,   60,
       $END
```

INITIAL DISTRIBUTION LIST

		No. Copies
1.	Defence Technical information Center Cameron Station Alexandria VA 22304-6145	2
2.	Library, Code 052 Naval Postgraduate School Monterey CA 93943-5002	2
3.	Chairman Department of Aeronautics, Code AA/Co Naval Postgraduate School Monterey CA 93943-5000	1
4.	Prof. Oscar Biblarz Department of Aeronautics, Code AA/Bi Naval Posgraduate School Monterey CA 93943-5000	3
5.	Prof. Garth Hobson Department of Aeronautics, Code AA/Hg Naval Postgraduate School Monterey CA 93943-5000	1
6.	Prof. Josef Rom c/o Prof Biblarz Department of Aeronautics, Code AA/Bi, NPS Monterey CA 93943-5000	1
7.	Dr. Craig Porter Naval Weapon Center, Code 3591 China Lake CA 93555	1
8.	Mr. James L. Hunt Ms 350 Langley Res. Center Hampton VA 23665-5225	1
9.	Major Eddy Priyono Dislitbangau, Lanud Husein S. Bandung, Indonesia	3